NORDITA

Nordic Institute for Theoretical Physics

Stockholms universitet

The growth of waves by wind as a problem in nonequilibrium statistical mechanics

Anthony Bonfils

Akademisk avhandling för avläggande av licentiatexamen vid Stockholms universitet, Fysikum

Mars 2020

The growth of waves by wind as a problem in nonequilibrium statistical mechanics

Anthony Bonfils

Abstract:

In 1948, Casimir predicted a net attractive force between two perfectly conducting parallel plates due to electromagnetic vacuum fluctuations. By analogy, the interaction of two ships on a wavy sea has been named Maritime Casimir effect. This is an example of force generation in non-equilibrium systems. Lee, Vella and Wettlaufer showed it to be oscillatory as it is induced by the sharply peaked energy spectrum measured in the sixties by Pierson and Moskowitz for a fully developed sea; a sea whose state is independent of the distance over which the wind blows and the time for which it has been blowing. The aim of this project is to construct a theory for that spectrum and understand how the Maritime Casimir effect emerges from wind-wave interaction. Waves in the absence of wind, so-called water waves, are mainly characterized by dispersion and weak non-linearity. The coupling of both results in the instability of a wave packet to side-band perturbations in deep water. The growth rate can be calculated thanks to a non-linear Schrödinger equation, which is a universal model for weakly non-linear waves in a dispersive medium. Furthermore, this instability can be understood in the even more general framework of resonant wave-wave interaction. The evolution of deep water gravity waves is actually a sum of four-wave interaction processes and triadic interactions should be added for capillary waves. That evolution is strongly affected by the presence of turbulent wind because it transfers energy to the waves. The growth rate of wind waves was calculated by Miles in 1957 on the basis of the weak air-water coupling. His formula involves the solution of the hydrodynamic Rayleigh equation at the critical level, which is the height at which the phase speed of the wave is equal to the wind speed. We develop an efficient numerical scheme to compute it and then compare the theory with the observational data compiled by Plant. We eventually propose asymptotic solutions of the Rayleigh equation for a generic wind profile, which will be useful to get a better understanding of the experimental results.

Akademisk avhandling för avläggande av licentiatexamen vid Stockholms universitet, Fysikum

Licentiatseminariet äger rum 17 mars 2020 kl. 13:30 i sal 112:028, Nordita South building, Roslagstullsbacken 11, Stockholm.

Acknowledgements

First of all, I wish to thank my main advisor Prof John Wettlaufer for his ‘subtle and subdued’ supervising; I guess he will recognize those words. The opportunity he gave me to do research in theoretical physics has no price to my eyes. Furthermore, I am grateful for the freedom he let me to choose my own directions and also to do the inevitable mistakes necessary to progress. Then, many thanks go to Dr Woosok Moon and Dr Dhrubaditya Mitra for their availability and wise advice. Their help has been particularly precious in the development of my numerics. I am also thankfull to all people at Nordita for making it such a pleasant working place. I am aware that I have been extremely lucky to have the possibility to travel so much and attend various workshops, conferences and schools, so I acknowledge the support from Swedish Research Council Grant 638-2013-9243. In addition, I wish to thank Prof Edwin Langmann for reading my manuscript and Dr Kristian Gustafsson for being my opponent. Last but not least, I thank my parents for their inconditional support and love.

Contents

Chapter 1

Motivation: the oscillatory Casimir effect

1.1 Introduction

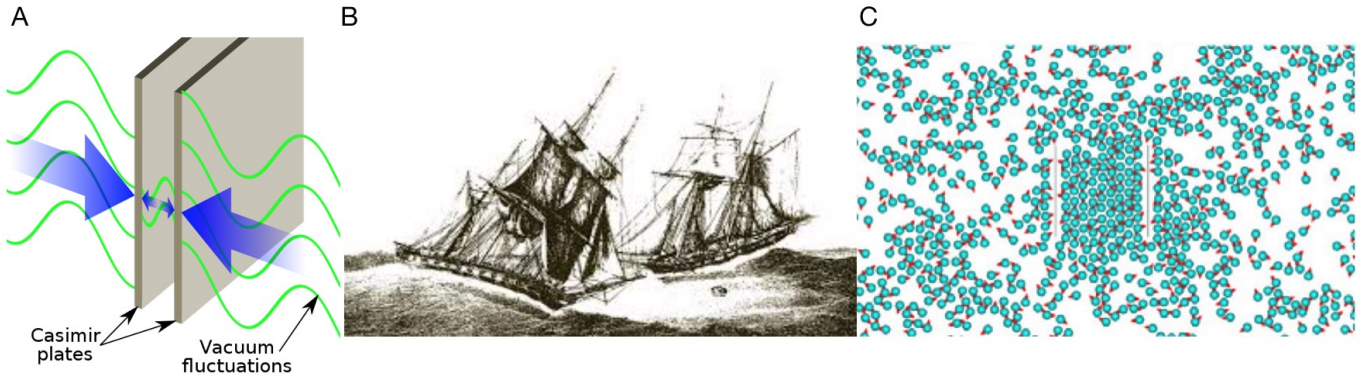

Figure 1.1: A) Original Casimir effect, adapted from Wikipedia.
B) Maritime Casimir effect, adapted from *L'Album du Marin* (1836) by P. C. Caussée.
C) Force generation between plates in active matter, adapted from [2].

The motivation for this project is the understanding of force generation in non-equilibrium systems, which is a significant challenge in statistical and biological physics, as well as a stumbling block in the development of active materials. A key to force generation in non-equilibrium systems is encoded in their energy fluctuation spectra $G(k)$ defined from the mean energy E as

$$E = \int_0^{+\infty} G(k)dk, \tag{1.1}$$

for one-dimensional systems. A non-equipartition of energy, which is only possible in active or driven systems, can lead to a non-monotonic fluctuation spectrum. Lee et. al [1] have recently shown that for a narrow, unimodal spectrum, the force exerted by a non-equilibrium system on two walls embedded in a system with such a spectrum depends solely on the width and the position of the peak in the fluctuation spectrum, and oscillates between repulsion and attraction as a function of wall separation. This is reminiscent of the Casimir effect in electrodynamics, except that the latter is always attractive. The theory developed in [1] predicts an oscillatory interaction between two ships on a wavy sea, and hence an oscillatory Maritime Casimir effect. Furthermore, it is consistent with recent simulations of active Brownian particles [2].

In section 1.2, we reproduce the original calculation of the Casimir force in electrodynamics. Then, we show

in section 1.3 how to generalize it to plates immersed in a non-equilibrium system thanks to a radiation stress tensor, before applying it to a simple model of ships on a wavy sea.

1.2 Casimir's original calculation

Let us consider two perfectly conducting parallel plates of identical area $\mathcal{A}$, at temperature $T = 0$, separated by a distance L. The x-axis is taken orthogonal to the plates; one plate is located at $x = 0$, the other at $x = L$. In this section, c denotes the speed of light in vacuum.

The Casimir force can be inferred up to a numerical factor thanks to an elementary analysis:

$$F_{cas} \propto \mathcal{A}\frac{\hbar c}{L^4}, \tag{1.2}$$

where $\hbar$ is the reduced Planck constant. We now outline the original calculation of Casimir [3].

Let us introduce the vector potential $\boldsymbol{A}(\boldsymbol{r}, t)$; there is no electric potential in the absence of source charge. In the Coulomb gauge, defined by $\boldsymbol{\nabla} \cdot \boldsymbol{A} = 0$, the electromagnetic field is then $\boldsymbol{E} = -\frac{1}{c}\partial_t \boldsymbol{A}$ and $\boldsymbol{B} = \boldsymbol{\nabla} \times \boldsymbol{A}$.

In the case of free fields, Maxwell's equations are equivalent to the homogeneous D'Alembert equation for the vector potential. Considering monochromatic waves, $\boldsymbol{A}(\boldsymbol{r}, t) = \tilde{\boldsymbol{A}}(\boldsymbol{r})\, e^{-i\omega t}$ and D'Alembert equation is reduced to the Helmholtz equation in the amplitudes:

$$\nabla^2 \tilde{\boldsymbol{A}} + \left[\frac{\omega}{c}\right]^2 \tilde{\boldsymbol{A}} = \boldsymbol{0}. \tag{1.3}$$

The electromagnetic field can also be regarded as a quantum harmonic oscillator whose energy levels are

$$E_m = \hbar\omega\left(m + \frac{1}{2}\right), \qquad m \in \mathbb{N}. \tag{1.4}$$

Between the plates, modes are quantized in the x-direction as a result of the confinement, like standing waves on a string. More precisely, since the tangential component of the electric field has to vanish at the boundary of a perfect conductor, we have

$$\tilde{\boldsymbol{A}}^{\parallel}(x = 0, y, z) = 0 \qquad \text{and} \qquad \tilde{\boldsymbol{A}}^{\parallel}(x = L, y, z) = 0, \qquad \forall\, y, z. \tag{1.5}$$

In this section, the symbol $\parallel$ means parallel to the plates. The normal component of the electric field should be finite at the boundary of a perfect conductor as it sets up a superficial density of charges. Separating x from other variables in Helmholtz equation (1.3) and imposing (artificial) periodic boundary conditions in the y and z-directions, we readily find

$$\tilde{\boldsymbol{A}}^{\parallel} \propto e^{i\boldsymbol{k}^{\parallel}\cdot\boldsymbol{r}^{\parallel}} \sin\left(\frac{n\pi}{L}x\right) \boldsymbol{e}_\lambda \qquad \text{and} \qquad \tilde{A}_x \propto e^{i\boldsymbol{k}^{\parallel}\cdot\boldsymbol{r}^{\parallel}} \cos\left(\frac{n\pi}{L}x\right), \qquad n \in \mathbb{N}, \tag{1.6}$$

where $\boldsymbol{e}_\lambda$ is a unit vector parallel to the plates defining the polarization and

$$\boldsymbol{k}^{\parallel} = n_y \frac{2\pi}{L_y}\, \boldsymbol{e}_y + n_z \frac{2\pi}{L_z}\, \boldsymbol{e}_z, \qquad n_y, n_z \in \mathbb{Z}, \tag{1.7}$$

where L_y and L_z are the sizes of the plates. Therefore, the energy inside the cavity is equal to

$$E_0 = \frac{1}{2}\sum_{n,\boldsymbol{k}^{\parallel}} \hbar\omega_n\big(\boldsymbol{k}^{\parallel}\big) \qquad \text{with} \qquad \omega_n\big(\boldsymbol{k}^{\parallel}\big) = c\sqrt{\frac{n^2\pi^2}{L^2} + |\boldsymbol{k}^{\parallel}|^2}. \tag{1.8}$$

A few points still have to be emphasized.

1. The gauge condition $\boldsymbol{\nabla}\cdot\tilde{\boldsymbol{A}}=0$ determines the polarization:

$$\frac{n\pi}{L}\tilde{A}_x+\boldsymbol{k}^{\parallel}\cdot\tilde{\boldsymbol{A}}^{\parallel}=0. \tag{1.9}$$

When $n\neq 0$, there exists two unit vectors $\boldsymbol{e}_1$ and $\boldsymbol{e}_2$ such that this condition is satisfied together with

$$\boldsymbol{e}_1\cdot\boldsymbol{e}_2=0 \qquad \text{and} \qquad \boldsymbol{e}_\lambda\cdot\boldsymbol{e}_x=0, \qquad \lambda=1,2. \tag{1.10}$$

There are two independent states of polarization. However, when $n=0$ we should necessarily have $\boldsymbol{e}_\lambda$ in the direction of $\boldsymbol{k}^{\parallel}$, implying a single state of polarization. To take this into account, we hence introduce a factor 2 but denote the sum with a prime to specify that it has to be removed when $n=0$.

2. For sufficientlty large plates, n_y and n_z can be treated as continuous variables and the sum over $\boldsymbol{k}^{\parallel}$ replaced by the integral $\frac{L_yL_z}{(2\pi)^2}\int_{\mathbb{R}^2}dk_xdk_y$.

3. The sum over n is divergent. However, the assumption of a perfect conductor breaks down at short wavelengths, say smaller than the Bohr radius. High frequencies are then cut off from a large value ω_c with the help of a regularizing function χ such that

$$\chi(0)=1 \qquad \text{and} \qquad \chi\left(\frac{\omega_n(\boldsymbol{k}^{\parallel})}{\omega_c}\right)\xrightarrow[\omega_c\,\to\,+\infty]{}1. \tag{1.11}$$

Equation (1.8) eventually becomes

$$E_0=\frac{\mathcal{A}}{(2\pi)^2}{\sum_{n=0}^{+\infty}}'\int_{\mathbb{R}^2}dk_xdk_y\;\hbar\omega_n\big(\boldsymbol{k}^{\parallel}\big)\chi\left(\frac{\omega_n(\boldsymbol{k}^{\parallel})}{\omega_c}\right). \tag{1.12}$$

Assuming isotropy, $dk_xdk_y=\frac{2\pi}{c^2}\omega d\omega$. Then, we obtain the energy of interaction of the plates due to the modes between them as

$$E_0=\mathcal{A}\frac{\hbar}{2\pi c^2}{\sum_{n=0}^{+\infty}}'\int_{\omega_n(\boldsymbol{0})}^{+\infty}d\omega\;\omega^2\chi\left(\frac{\omega}{\omega_c}\right), \tag{1.13}$$

whose only dependence on L is through $\omega_n(\boldsymbol{0})=\frac{n\pi c}{L}$. The corresponding force is

$$F_{in}=-\frac{\partial E_0}{\partial L}=-\mathcal{A}\frac{\hbar c\pi^2}{2L^4}{\sum_{n=0}^{+\infty}}'n^3\chi\left(\frac{\omega_n(\boldsymbol{0})}{\omega_c}\right). \tag{1.14}$$

The force due to outside modes, which are not confined, is just the opposite of this one with the sum being replaced by an integral. The net force is then

$$F_{cas}=F_{in}+F_{out}=-\mathcal{A}\frac{\hbar c\pi^2}{2L^4}\left\{{\sum_{n=0}^{+\infty}}'n^3\chi\left(\frac{\omega_n(0)}{\omega_c}\right)-\int_0^{\infty}n^3\chi\left(\frac{\omega_n(0)}{\omega_c}\right)dn\right\}. \tag{1.15}$$

Finally, using the Euler-MacLaurin formula

$${\sum_{n=0}^{+\infty}}'g(n)-\int_0^{\infty}g(n)dn=-\frac{1}{12}g'(0)+\frac{1}{6!}g'''(0)+O\Big(g^{(5)}(0)\Big), \tag{1.16}$$

yields the attractive force

$$F_{cas}=-\mathcal{A}\frac{\hbar c\pi^2}{240L^4}. \tag{1.17}$$

We note that his result has also been derived by Milonni et al. using a radiation pressure [4].

1.3 Oscillatory force generation from peaked energy spectrum

This section is based on the paper [1] *by Lee, Vella and Wettlaufer.*

We consider now out-of-equilibrium systems where the fluctuations are manifested as one-dimensional waves with wavenumber vector $\boldsymbol{k}$. Assuming no dispersion, the corresponding radiation stress tensor is

$$\mathbb{\Pi} = G(k)\,\hat{\boldsymbol{k}} \otimes \hat{\boldsymbol{k}}, \qquad \hat{\boldsymbol{k}} = \frac{\boldsymbol{k}}{|\boldsymbol{k}|}. \tag{1.18}$$

To be consistent with the definition (1.1), we have taken the point of view that the waves propagate only forwards so that $k = |\boldsymbol{k}|$.

Let us embed two walls separated by a distance L within such a system. The fluctuations due to the out-of-equilibrium state will play the same role as the vacuum fluctuations in the original Casimir effect. From (1.18), a wave having a wavelength $\frac{2\pi}{k}$ and an angle of incidence θ induces a radiation pressure $G(k)\cos^2(\theta)$. Thus, the radiation force per unit angle due to waves with a wavenumber between k and $k + \delta k$ and reflecting with an angle between θ and $\theta + \delta\theta$ is [1]

$$\delta F = G(k)\delta k \cos^2(\theta)\frac{\delta\theta}{2\pi}. \tag{1.19}$$

As in the previous section, there are standing waves between the plates which imposes mode quantization while there is a continuum acting on the exterior of the plates. For isotropic fluctuations, we integrate θ from $-\frac{\pi}{2}$ to $\frac{\pi}{2}$ and eventually get the net disjoining force

$$F_{fluct}(L) = \frac{1}{4}\sum_{n=1}^{\infty}\frac{\pi}{L}\,G\left(\frac{n\pi}{L}\right) - \frac{1}{4}\int_0^{\infty} G(k)dk. \tag{1.20}$$

Note that

$$\frac{dG}{dk} \lesseqgtr 0, \quad \forall k \qquad \Rightarrow \qquad F_{fluct}(L) \lesseqgtr 0, \quad \forall L. \tag{1.21}$$

Therefore, a non-monotonic force implies a non-monotonic spectrum. This is important for systems whose spectrum is not known theoretically but for which one can observe an oscillatory force due non-equilibrium interactions. The reason is that the latter are indeed encoded within the fluctuation spectrum. 'In this sense, the noise becomes the signal'.

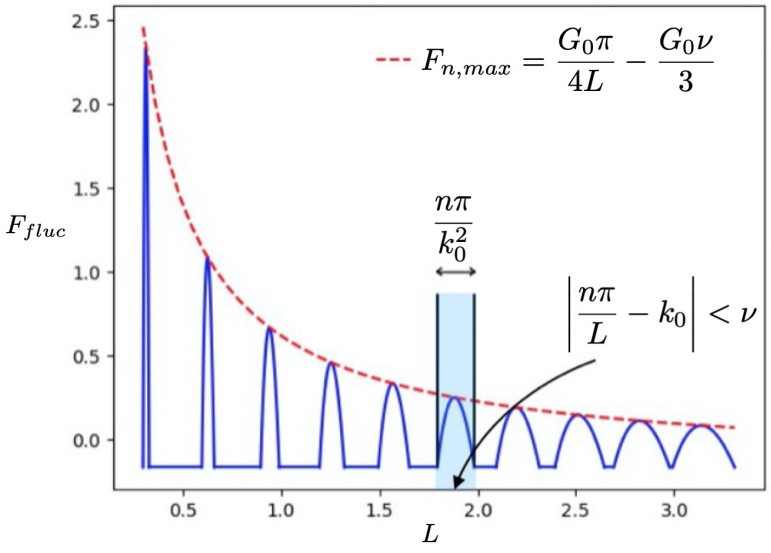

Figure 1.2: Oscillatory force induced by a unimodal spectrum modeled by equation (1.22). It depends only on the width and the position of the peak.

[1] δF is actually a force per unit length as G has the dimension of a force in this effectively one-dimensional system.

Furthermore, it can be shown that unimodal spectra have a universal phenomenology, and can be represented by a Taylor expansion about their maximum at $k = k_0$:

$$G(k) \simeq \begin{cases} G_0 \left[1 - \nu^{-2}(k-k_0)^2\right], & |k-k_0| < \nu \\ 0 & \text{otherwise,} \end{cases} \tag{1.22}$$

where $G_0 = G(k_0)$, $G_2 = G''(k_0)$ and $\nu = \sqrt{-2\frac{G_0}{G_2}}$ is the peak width. The following asymptotic scalings are derived in [1]:

1. For $L \ll \frac{\pi}{\nu}$ and in the narrow-peak limit $\nu \ll k_0$, the force has successive repulsive peaks scaling as $\frac{1}{L}$, with linearily increasing width (proportional to their index n) as the distance L gets larger and larger. See figure 1.2.
2. For $L \gg \frac{\pi}{\nu}$, one can show with the help of the Euler-MacLaurin formula (1.16) that the force scales as $\frac{1}{L^2}$. This actually holds for a spectrum that is not necessarily unimodal.

Application to the Maritime Casimir effect

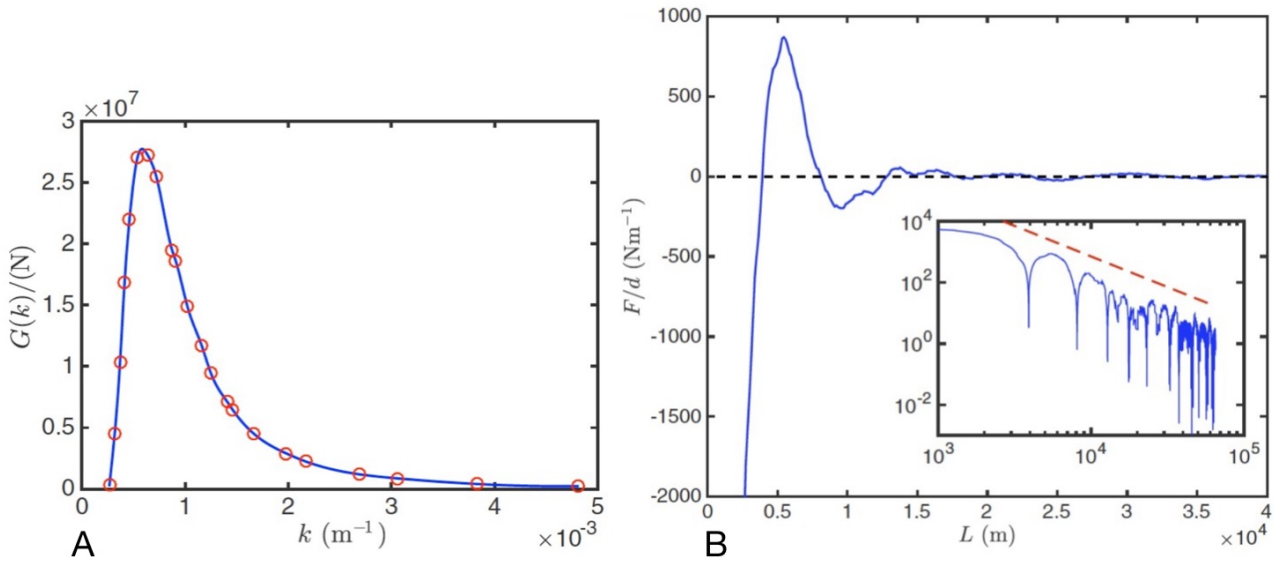

Figure 1.3: A) Pierson&Moskowitz spectrum; the data points (red circles) are fitted with a cubic spline.
B) Force induced by that spectrum on two "ships"; the dashed red line corresponds to the asymptotic scaling $\frac{1}{L^2}$.
Figures adapted from [1].

These results shed light on the old riddle of the Maritime Casimir effect. Indeed, the framework we have just described can be taken as a simple model for two ships on the sea with the wind blowing in a direction perpendicular to them. The ocean wave spectrum was measured in 1964 by Pierson and Moskowitz [5] for a fully developed sea, which corresponds to an out-of-equilibrium steady state where the wave-wave interactions are balanced by the wind input and dissipation through wave breaking. The force between the two ships calculated from formula (1.20) using that spectrum oscillates between attraction and repulsion depending on the distance separating them.

Chapter 2

The physics and mathematics of waves and how they grow under the wind blowing

In this chapter is introduced some background about ocean waves. In section 2.1, we review the water wave problem by taking a historical perspective and show that dispersion and weak non-linearity are nicely treated in the framework of wave-wave interactions. Ocean waves are water waves coupled with the wind. We provide in section 2.2 a brief history of the proposed mechanisms for wind waves' generation before focusing on the Miles' theory, as it is the core of our research presented in chapter 3.

2.1 Water waves: dispersive and weakly non-linear waves

2.1.1 Cauchy-Poisson problem and Airy linear theory

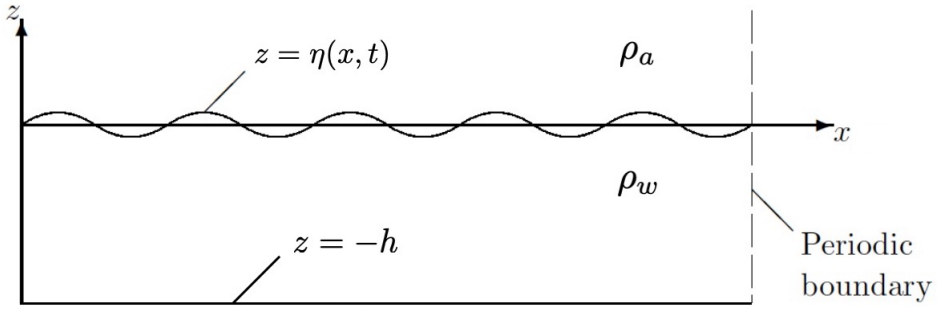

Figure 2.1: Schematic of the water wave problem in 2 dimensions where η is the surface displacement field about the equilibrium position $z = 0$; ρ_a and ρ_w are the densities of air and water, and h the water depth.

Water waves are as fascinating as they are ubiquitous. One can observe them by a windy day on the surface of ponds, lakes, rivers, oceans… Their ever-changing pattern, endless succession of humps and hollows, has attracted the attention of scientists and sailers for centuries. Their mathematical study started in France with the prize competition on "The theory of the propagation of Waves, at the surface of a heavy fluid, of indefinite depth" proposed by the French Academy of Sciences in December 1813 [6]. Cauchy won the prize but Poisson, who was one of the examiners, also published his own work on the topic. They determined the waves created by a sudden disturbance η at the air/water interface $z = 0$, what became the so-called Cauchy-Poisson problem. They considered an inviscid irrotational and incompressible flow so that they had to solve the Laplace equation

with a deformable boundary[1] $z = \eta(x, y, t)$. Assuming an infinitesimal 2-dimensional disturbance, the boundary conditions were linearized about the unperturbed water surface $\eta(x, y, t) = 0$. However, they still had to face the major issue of dispersion: waves with different wavelengths propagate at different speeds. Indeed, if one tries to follow one of the ripples created when throwing a stone into water, one shortly looses it because it is caught up by others. Cauchy and Poisson independently derived the dispersion relation of deep water gravity waves: $\omega = \sqrt{g|\boldsymbol{k}|}$ where ω is the angular frequency, g the gravitational acceleration and $\boldsymbol{k}$ the wavenumber vector. In a modern view, they decomposed the initial disturbance $\eta(x, y, t = 0)$ into Fourier modes, imposed a linear evolution and obtained its shape at later times through an inverse Fourier tranform:

$$\eta(x, y, t) = \frac{1}{(2\pi)^2} \iint_{\mathbb{R}^2} \hat{\eta}(k, l)\, e^{i[kx+ly-\omega(k,l)t]}\, dkdl \quad \text{with} \quad \hat{\eta}(k, l) = \iint_{\mathbb{R}^2} \eta(x, y, t = 0)\, e^{-i(kx+ly)}\, dxdy. \tag{2.1}$$

Although their results on the interference of Fourier modes in a dispersive medium are one the greatest scientific achievements of their time, they were regarded as a mathematical curiosity. In fact, the physical theory of linear water waves was provided by Airy in 1841 [8]. Waves are perturbations of the water surface and they propagate due to a restoring force: gravity and/or surface tension, denoted σ. Moreover, one can classify them in terms of the water depth h. For the sake of simplicity, we will focus on a 2-dimensional problem (1-dimensional waves, see figure 2.1). The general dispersion of capillary-gravity waves in a layer of finite depth is then [9]

$$\omega^2 = gk \tanh(kh)\left(1 + \frac{\sigma k^2}{\rho_w g}\right), \qquad k = |\boldsymbol{k}|, \tag{2.2}$$

where ρ_w is the density of water. The capillary wave length is defined as $\lambda_c = 2\pi\sqrt{\frac{\sigma}{\rho_w g}} \simeq 1.7\ cm$. For wavelengths much smaller than λ_c, surface tension is the only restoring force. Conversely, for wavelengths much greater than λ_c only gravity matters. Shallow water waves are defined by $kh \ll 1$ and, given λ_c, such waves cannot be capillary. Furthermore, their phase velocity $c = \frac{\omega}{k}$ is constant equal to $\sqrt{gh}$, so they are not dispersive. We will not be concerned with shallow water waves in this work. We will actually focus on the other limiting case, $kh \gg 1$, corresponding to the so-called deep water waves. Their phase velocity is minimal at the capillary wavenumber $k_c = \sqrt{\frac{\rho_w g}{\sigma}}$ and can be expressed as

$$c = \frac{c_{min}}{\sqrt{2}} \sqrt{\frac{k}{k_c} + \frac{k_c}{k}}, \qquad \text{with} \qquad c_{min} = \left(\frac{4\sigma g}{\rho_w}\right)^{\frac{1}{4}}. \tag{2.3}$$

The neglect of surface tension gives back the result of Cauchy and Poisson, $c = \sqrt{\frac{g}{k}}$, which is subsequently correct for $k \ll k_c$.

2.1.2 Stokes' non-linear step

Much of the zoology of water waves and how they propagate is therefore well understood. However, the framework we have just described holds under the assumption that waves have an infinitesimal amplitude, whatever their origin. In this work, we will be concerned with wind-generated waves. But when a strong wind is blowing, it creates big waves sometimes so big that they break, for the greatest pleasure of surfers, because the local downward acceleration of fluid particles exceeds the value of g; a phenomenon reported for the first time in a scientific journal by Phillips in 1958 [10]. Therefore, non-linear effects should definitely be taken into account. Their first study is due to Stokes for deep water gravity waves. In a seminal paper published in 1847 [11], he showed that, in addition to their oscillatory motion, fluid particles are also advected by the flow in the direction of wave propagation, so that they do not exactly have closed trajectories. This phenomenon is known to people who practice tackle fishing in the ocean; they indeed experience a drift of their fishing float and even of their boat, if they forgot to anchor it. This is referred to as Stokes drift, which mathematically corresponds to the difference between the mean Lagrangian and Eulerian velocities:

$$\boldsymbol{u}_S(\boldsymbol{r}_0) = \left\langle \frac{\partial \boldsymbol{\xi}(\boldsymbol{r}_0, t)}{\partial t} \right\rangle - \langle \boldsymbol{u}(\boldsymbol{r}_0, t) \rangle = \left\langle \left[\int_{t_0}^{t} \boldsymbol{u}(\boldsymbol{r}_0, t')dt' \cdot \boldsymbol{\nabla}_{\boldsymbol{r}_0} \right] \boldsymbol{u}(\boldsymbol{r}_0, t) \right\rangle, \tag{2.4}$$

[1] Laplace was contemporary of Cauchy and Poisson, but the eponymous equation was first introduced in hydrodynamics by Euler in 1761 [7].

where $\boldsymbol{\xi}(\boldsymbol{r}_0, t)$ denotes the position at time t of a fluid particle located in $\boldsymbol{r}_0$ at the initial time t_0. For a plane wave $\eta(x,t) = a\ \cos(kx - \omega t)$, Stokes obtained

$$\boldsymbol{u}_S(\boldsymbol{r}_0) = (ka)^2 \sqrt{\frac{g}{k}}\ e^{2kz_0}\ \boldsymbol{e}_x \qquad \text{for} \qquad ka \ll 1, \tag{2.5}$$

where $ka \equiv s$ is called the wave steepness. This dimensionless parameter, also known as the wave slope, characterizes the non-linearity of the waves. As Stokes masterfully noticed, $s \ll 1$ most of the time, so water waves are actually weakly non-linear. Note that the Stokes drift is nevertheless a key process in the transport of marine debris such as driftwood.

In the same article [11], Stokes used what is now called the Poincaré-Lindstedt method to derive a non-linear dispersion relation for deep water gravity waves of small steepness, now known as the Stokes waves:

$$\omega_S^2 = gk\big(1 + s^2\big), \qquad s \ll 1. \tag{2.6}$$

Thus, Airy linear theory for deep water waves is valid[2] in the limit $s \to 0$.

2.1.3 Modulational instability of a wave packet: NLS model

Stokes made a first step by deriving a dispersion relation that depends on the wave amplitude, but the evolution of that amplitude was still unknown. The existence of Stokes waves was rigorously proved by Levi-Civita in 1925 [12], however such non-linear periodic wave trains are rarely observed in nature. In fact, Benjamin and Feir showed in 1967 [13], both experimentally and analytically, that they are unstable to side-band perturbations: a Stokes wave of wavenumber k_0 is usually accompanied by residual perturbations of wavenumber, say $k_\pm = k_0 \pm \Delta k$ with $\Delta k \ll k_0$, and it turns out that those perturbations grow exponentionally, causing the disintegration of the Stokes wave. From this observation naturally arises the question of how the interaction between dispersion and weak non-linearity affects the propagation of a narrow wave packet centered around k_0. The simplest answer is given by an envelope equation. The wave packet is represented by a surface displacement of the form [14]

$$\eta(x,t) = \Re\Big\{ A(x,t)\ e^{i(k_0 x - \omega_0 t)} \Big\}, \qquad \text{with} \qquad \omega_0 = \sqrt{gk_0}. \tag{2.7}$$

The condition of narrow spectral band-width, $\delta = \frac{\Delta k}{k_0} \ll 1$, is equivalent to the complex wave amplitude being slowly varying in space. Then, the latter is the solution of

$$i\left(A_t + \frac{\omega_0}{2k_0}\ A_x\right) = \frac{\omega_0}{8k_0^2}\ A_{xx} + \frac{1}{2}\omega_0 k_0^2\ |A|^2 A. \tag{2.8}$$

This is a non-linear Schrödinger equation (NLS), which can be obtained using the method of multiple scale on the water wave equations. We are going to highlight the general physical processes it describes. First, let us remark that $\frac{\omega_0}{2k_0} = \omega'(k_0) \equiv c_{g0}$ is the group velocity of the waves evaluated at k_0; the propagation of the envelope of a wave packet at the group velocity is a well-known result. So if we write equation (2.8) in a moving frame defined as $\xi = x - c_{g0}t$ and $\tau = t$, the second term on the left-hand side disappears. Furthermore, let us temporarily ignore the spatial dependence in the new frame. Hence,

$$iA_\tau = \frac{1}{2}\omega_0 k_0^2\ |A|^2 A. \tag{2.9}$$

Because the modulus of the solution $|A|$ is constant in time, one readily finds $A(\tau) = A_0\ e^{-i\Omega\tau}$, where $\Omega = \frac{1}{2}\omega_0\big(k_0|A_0|\big)^2$ is simply the Stokes' correction. Since Stokes considered a plane wave, he was indeed right to presuppose a constant wave amplitude. The condition of weak non-linearity can be imposed by the transformation $A \to sA$. Then, the non-linear effects clearly occur on a time scale of order s^{-2}.

Let us now give a heuristic derivation of the linear part of equation (2.8) for an arbitrary dispersion relation. The initial condition must be a slow function of x, meaning that $A(x,0) = f(\delta x)$. After expanding it in a Fourier integral, the linear evolution of the wave packet is given by

$$\eta(x,t) = \Re\left\{ \frac{1}{2\pi} \int_{-\Delta k}^{\Delta k} \hat{A}(k)\ e^{i[(k_0+k)x - \omega(k_0+k)t]}\ dk \right\}. \tag{2.10}$$

[2]For waves in finite depth, Airy linear theory is valid if in addition $a \ll h$. Futhermore, for shallow water waves the Ursell number $Ur = \frac{a}{k^2h^3}$ must also be very small.

Because $\delta \ll 1$, we have $k \ll k_0$ and hence we can Taylor-expand the dispersion relation about k_0. After comparison with (2.7), we find

$$A(x,t) = \frac{1}{2\pi}\int_{-\Delta k}^{\Delta k} \hat{A}(k)\, e^{i\left[kx-\left(\omega'(k_0)k+\omega''(k_0)\frac{k^2}{2}+\dots\right)t\right]}\, dk, \tag{2.11}$$

which obeys

$$i\big(A_t + \omega'(k_0)\, A_x\big) = -\frac{1}{2}\omega''(k_0)\, A_{xx}. \tag{2.12}$$

For deep water gravity waves, we effectively have $\omega''(k_0) = -\frac{\omega_0}{4k_0^2} < 0$. We will see that the concavity of the function $\omega(k)$ is of primary importance. Let us emphasize that to have a balance between the different terms, the complex amplitude must be a slow function of t. There are actually two time scales. The envelope propagates on a time scale of order δ^{-1} and gets distorted on a time scale of order δ^{-2}.

To summarize, let us combine the conclusions by rewriting the wave packet as

$$\eta(x,t) = \Re\Big\{ sA(\xi,\tau)\, e^{i(k_0x-\omega_0t)}\Big\}, \qquad \text{with} \qquad \begin{cases}\xi = \delta(x-c_{g0}t)\\ \tau = \delta^2 t\end{cases}. \tag{2.13}$$

This way, the scale separation is properly accounted for and the balance between dispersion and weak non-linearity becomes transparent:

$$i\delta^2 A_\tau = -\frac{\delta^2}{2}\omega''(k_0)\, A_{xx} + \frac{s^2}{2}\omega_0 k_0^2\, |A|^2 A. \tag{2.14}$$

When $\delta \ll s \ll 1$ non-linearity dominates dispersion and the wave-packet behaves like a uniform wave train whose phase velocity depends on its amplitude. On the contrary, for $s \ll \delta \ll 1$ the propagation of the wave packet is perfectly linear but fully dispersive, treated in a general manner. We will see that the form of the non-linear term is not specific to water waves. Thus, the NLS is a general model for waves displaying $\delta \sim s \ll 1$. Let us show that it explains the Benjamin-Feir instability, which is why it is often called the modulational instability [15]. Still working in the moving frame, we perturb the Stokes' solution as follows:

$$A(\xi,\tau) = \big[A_0 + B(\xi,\tau)\big]\, e^{-i\Omega\tau}, \qquad \text{with} \qquad B \ll A_0. \tag{2.15}$$

Since we are interested in side-band perturbations, we write $B(\xi,\tau) = B_+\, e^{i\Delta k\xi+\gamma\tau} + B_-\, e^{-i\Delta k\xi+\gamma^*\tau}$ where γ is the possibly complex growth rate to be determined and $(B_+, B_-) \in \mathbb{C}^2$. The algebra, detailed in reference [16], results in

$$\gamma^2 = -\frac{\Delta k^2}{4}\Big\{2\omega''(k_0)\big(k_0|A_0|\big)^2 + \big[\omega''(k_0)\big]^2\Delta k^2\Big\}. \tag{2.16}$$

We immediately notice that this square is non-negative only if $\omega''(k_0) < 0$, thereby revealing that concavity of the dispersion relation is a necessary condition for side-band instability. However, this is not sufficient because it also has a threshold. For deep water gravity waves, the dimensionless growth rate can be written as

$$\frac{\gamma}{\omega_0} = \frac{1}{8}\delta\sqrt{8s^2-\delta^2}, \tag{2.17}$$

so that $\delta < 2\sqrt{2}s$ is required for growth, which is maximal at $\delta = 2s$.

2.1.4 Wave-wave interaction

The mechanism of the Benjamin-Feir instability is well understood in the general framework of wave-wave interactions [17]. In fact, the carrier wave is interacting with the side-bands in a resonant process characterized by

$$\begin{cases} k_0 + k_0 = k_0 + \Delta k + k_0 - \Delta k\\ \omega(k_0) + \omega(k_0) = \omega(k_0+\Delta k) + \omega(k_0-\Delta k)\end{cases}. \tag{2.18}$$

The condition on frequencies is clearly not fullfilled when using the linear dispersion relation $\omega_L(k) = \sqrt{gk}$. But since we are dealing with waves of small but finite steepness, we should use a non-linear dispersion relation. For

the carrier wave, we directly apply Stokes' result: $\omega(k_0) = \omega_0\left(1 + \frac{s^2}{2}\right)$. The side-bands suffer from non-linearity in a different way. Indeed, they are infinitesimal ($B \ll A_0$) but they are riding on the carrier wave, which sets up a Stokes drift. Evaluated here at the water surface, $z_0 = 0$, the latter is $u_S = c_0 s^2$ where $c_0 = \frac{\omega_0}{k_0}$. Due to this wave-induced current, the side-bands are Doppler-shifted:

$$\omega(k_0 \pm \Delta k) = \omega_L(k_0 \pm \Delta k) + (k_0 \pm \Delta k)u_S. \tag{2.19}$$

A Taylor expansion of ω_L at second order about k_0 shows that the condition on frequencies is fullfilled exactly for the side-bands yielding the maximum growth rate of the Benjamin-Feir instability. This is probably the best observational evidence of four-wave interactions. Such interactions are the consequence of dispersion and non-linearity. They are mathematically described by the Zakharov equation [18]

$$\frac{\partial a_1}{\partial t} + i\omega_1 a_1 = -is^2 \iiint_{\mathbb{R}^3} T_{1234}\, a_2^* a_3 a_4\, \delta(k_1 + k_2 - k_3 - k_4)\, dk_2 dk_3 dk_4, \tag{2.20}$$

where k_j denotes an algebraic wavenumber, $\omega_j = \omega_L(|k_j|)$, $T_{1234} = T(k_1, k_2, k_3, k_4)$ is a real scattering coefficient and $a_j = a(k_j, t)$ is a spectral amplitude related to the surface displacement by

$$\eta(x,t) = \frac{1}{2\pi} \int_{\mathbb{R}} \left[\frac{|k|}{4\rho_w g}\right]^{\frac{1}{4}} \{a(k,t) + a^*(-k,t)\} e^{ikx} dk. \tag{2.21}$$

Zakharov derived equation (2.20) using a perturbative Hamiltonian formalism based on the assumption of weak non-linearity of water waves. Since then, equations of the same form have been found for other systems of weakly non-linear waves. It displays a clear time scale separation: waves have a fast oscillatory dynamics while their amplitude is slowly varying because of wave-wave interaction. So if we define a 'slow' time $t_2 = s^2 t$ and $b(k,t) = a(k,t)e^{-i\omega_L(k)t}$, we get

$$\frac{\partial b_1}{\partial t_2} = -i \iiint_{\mathbb{R}^3} T_{1234}\, b_2^* b_3 b_4\, e^{i(\omega_1 + \omega_2 - \omega_3 - \omega_4)t} \delta(k_1 + k_2 - k_3 - k_4)\, dk_2 dk_3 dk_4. \tag{2.22}$$

First of all, the non-linear term of NLS straightforwardly emerges from this equation when considering a single mode which is basically interacting with itself. Secondly, it now appears obvious that the key processes are resonant four-wave interactions:

$$\begin{cases} k_1 + k_2 = k_3 + k_4 \\ \omega_1 + \omega_2 = \omega_3 + \omega_4 \end{cases}. \tag{2.23}$$

Phillips, who is actually the first to come up with the idea of wave-wave interaction, proved in 1960 [19] with

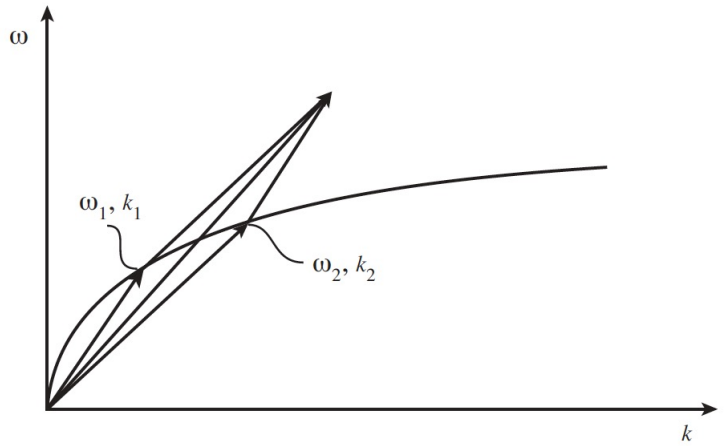

Figure 2.2: There is no resonant triadic interactions between deep water gravity waves because they cannot satisfy both $k_1 + k_2 = k_3$ and $\omega_1 + \omega_2 = \omega_3$. Figure adapted from [17].

his famous figure of eight that this system has solutions. Resonant triadic interactions are not possible because

ω_L is a concave functions, as can be graphically seen on figure 2.2; however, they are present when the surface tension is taken into account.

Finally, it is worth noticing that the originally cumbersome expression of T_{1234} has undergone numerous simplications over the last half-century, especially after the release of Wolfram. For 2-dimensional deep water gravity waves, its final expression is [20]

$$T_{1234} = \theta(k_1k_2k_3k_4)\,\frac{\sqrt{k_1k_2k_3k_4}}{4\pi}\left(\sqrt{\frac{\omega_1\omega_2}{\omega_3\omega_4}}+\sqrt{\frac{\omega_3\omega_4}{\omega_1\omega_2}}\right)\min(|k_1|,|k_2|,|k_3|,|k_4|), \tag{2.24}$$

where θ is the Heavide step function. Furthermore, the resonant manifold can very interestingly be decomposed into two branches:

$$\begin{cases} k_1 = k_3 \text{ and } k_2 = k_4 \\ \text{or} \\ k_1 = k_4 \text{ and } k_2 = k_3 \end{cases} \quad \text{and} \quad \begin{cases} k_1 = \alpha(1+\zeta)^2 \\ k_2 = \alpha\zeta^2(1+\zeta)^2 \\ k_3 = -\alpha\zeta^2 \\ k_4 = \alpha(1+\zeta+\zeta^2)^2 \end{cases}, \qquad \alpha \in \mathbb{R} \qquad \text{and} \quad \zeta \in]0,1[. \tag{2.25}$$

Then one can check with expression (2.24) that T_{1234} is identically zero on the second branch. So we come to the astonishing conclusion that there are only trivial resonant interactions in that case.

We close this broad introduction to the water wave problem with the emphasis that weak non-linearity is a key feature in its mathematical treatment. Stokes' expansion and the more general framework of wave-wave interaction make sense only because the steepness of the waves is small. The reason for it is the existence of a natural small parameter in the system: the air-water density ratio $\epsilon = \frac{\rho_a}{\rho_w}$. Water waves are strictly speaking interfacial waves, however the water surface has been treated as a free surface because $\epsilon \ll 1$. Indeed, it ensures a weak coupling between air and water layers, and subsequentlty $s \ll 1$. This is an essential fact for the study of wind-wave interaction.

2.2 Wind waves

2.2.1 Brief history of the generation of waves by the wind

The first mechanism for the generation of waves by the wind was proposed by Kelvin and Helmholtz around 1870. It was based on the instability of two layers of fluid having each a different velocity and now known as the vortex sheet instability. However, the minimum wind speed for this instability to occur is too large. So it cannot account for wind wave generation. Still the Kelvin-Helmholtz instability is ever-present in nature and of great importance in astrophysics.

It is only in 1925 that another mechanism was suggested by Jeffreys. He considered harmonic waves having a phase velocity c together with a constant wind speed U and noticed that the pressure on the windward face of a crest was greater than the pressure on the leeward face of that crest. Then he assumed that this pressure difference should be proportional to the wave slope. This is the so-called sheltering hypothesis:

$$\Delta P = \mathfrak{s}\,\rho_a(U-c)^2\,\eta_x, \tag{2.26}$$

where $\mathfrak{s}$ is named 'sheltering coefficient' and should be experimentally determined. The pressure asymmetry is supposed to be due to flow separation: the air flowing over a wave separates somewhere on the downwind side and reattaches on the upwind side of the next crest. Unfortunately, this mechanism turned out to be inefficient. Moreover, Banner and Melville showed in 1976 that waves do not separate unless they break [21].

In 1956, Ursell wrote a very influencial review on the topic of wind wave generation where he concluded that its current stage at that time was unsatisfactory [22]. As a consequence, a year later Phillips [23] and Miles [24] proposed two independent mechanisms. The latter actually explains the growth of infinitesimal perturbations under the wind blowing while the former details the generation of a spectrum of waves by a turbulent wind. Thus, those mechanisms appear to complete each other rather than being in competition. In this work, we will focus on the theory of Miles.

2.2.2 A focus on Miles' theory

Background: Instability of a parallel shear flow

Let us consider a parallel shear flow $\boldsymbol{U} = U(z)\,\boldsymbol{e}_x$ over a flat boundary of infinite extension located at $z = 0$. Assuming this flow inviscid and the absence of gravity, it is a trivial solution of the incompressible Euler equation, together with a constant pressure P. For the sake of simplicity, we take the density of the fluid constant. The equilibrium state is now perturbed infinitesimally:

$$\boldsymbol{u} = \boldsymbol{U} + \boldsymbol{u}', \qquad |\boldsymbol{u}'| \ll |\boldsymbol{U}|, \tag{2.27}$$

$$p = P + p', \qquad p' \ll P. \tag{2.28}$$

A normal mode analysis consists in looking for solutions of the perturbed state in the form

$$p'(\boldsymbol{r}, t) = \hat{p}(z)\, e^{i(kx+ly-ct)} \quad \text{and} \quad \boldsymbol{u}'(\boldsymbol{r}, t) = \begin{pmatrix} \hat{u}(z) \\ \hat{v}(z) \\ \hat{w}(z) \end{pmatrix} e^{i(kx+ly-ct)}. \tag{2.29}$$

After Squire theorem [25], to each 3-dimensional disturbance corresponds a more unstable one in 2 dimension. Therefore, one can take $l = 0$ and $\hat{v} = 0$. Then it can be shown that the perturbed vertical velocity is solution of the so-called Rayleigh equation:

$$(U - c)(\hat{w}_{zz} - k^2\hat{w}) - U_{zz}\,\hat{w} = 0. \tag{2.30}$$

Since the flow cannot penetrate the boundary, $\hat{w}(0) = 0$. Furthermore, the disturbance should vanish at infinity. This is an eigenvalue problem: one has to find for each mode k the complex phase velocity $c(k)$ such that these boundary conditions are satisfied.

Instability of a logarithmic profile over a layer of fluid

Miles addressed the problem of how the wind makes a deep water water gravity wave of infinitesimal steepness grow. His idea was to look at that wave as a perturbation of the air flow and then study the stability of the latter. The issue is of course that the wind is turbulent while all results of the theory of hydrodynamic stability are for laminar flows [25]. Miles worked around the problem by averaging the turbulent flow.

A turbulent shear flow over a rough boundary located at $z = 0$ can be represented by the law of the wall [26]:

$$\bar{u}(z) = \frac{u_\star}{\kappa}\,\ln\left(\frac{z}{z_0}\right), \qquad \text{for} \qquad z \gg z_0. \tag{2.31}$$

The overbar stands for time averaging, $\kappa = 0.4$ is the von Karman constant, $u_\star$ the friction velocity defined from the constant shear stress $\tau_0 = \rho_a u_\star^2$ and z_0 the roughness length, that is nothing but the height at which $\bar{u}$ would vanish if equation (2.31) was applicable down to this height. Indeed, it is not valid close to the boundary because of the effect of viscosity. When the time scale of turbulent fluctuations is much smaller than the period of the wave, it is still valid to use equation (2.31) as a wind profile. Moreover, so as to mimic a viscous sublayer it is extended down to the water surface in the form

$$U(z) = \frac{u_\star}{\kappa}\,\ln\left(1 + \frac{z}{z_0}\right). \tag{2.32}$$

Assuming that there is no wind-drift, $U(z) = 0$ for $z < 0$. Note that this profile is continuous at $z = 0$ so that there is no Kelvin-Helmholtz instability. Since the perturbation is coming from the interface, one should solve the Rayleigh equation both in air and water. Furthermore, at the moving boundary $z = \eta(x, t)$ one should have

$$w_a = w_w = \frac{d\eta}{dt} \qquad \text{and} \qquad p_a = p_w, \tag{2.33}$$

where $\frac{d}{dt}$ is the material derivative and, as previously, w is the vertical velocity, p the pressure. Nonetheless, there is now gravity so that it is the hydrostatic pressure $P_0 - \rho g z$ which is perturbed in each layer of fluid, $P_0 = p(z = 0)$ being an arbitrary constant. One introduces a perturbed stream function ψ' such that

$$u' = -\psi'_z \qquad \text{and} \qquad w' = \psi'_x, \tag{2.34}$$

and look for the normal modes $\psi'(\boldsymbol{r},t) = \hat{\psi}(z)\, e^{i(kx-ct)}$. It is straightforward that $\hat{\psi}$ obeys the Rayleigh equation (2.30). Along the same line, the wave is represented by $\eta(x,t) = a\, e^{i(kx-ct)}$ but the dispersion relation $c(k)$ is now unknown. In fact, the whole point is to calculate it and show that it has a non-zero imaginary part. Since $ka \ll 1$, the boundary conditions (2.33) can be linearized:

$$\hat{\psi}_a = \hat{\psi}_w = -ac \qquad \text{and} \qquad \hat{p}_a - \hat{p}_w = (\rho_a - \rho_w)ga \qquad \text{at} \qquad z = 0. \tag{2.35}$$

In the establishment of equation (2.30), the pressure has been eliminated through an expression in terms of $\hat{\psi}$ and U. It used to rewrite the second conditions as

$$\left[\rho\Big\{\hat{\psi}_z(U-c)^2 - \hat{\psi}\big(U_z(U-c)+g\big)\Big\}\right]_w^a = 0 \qquad \text{at} \qquad z = 0. \tag{2.36}$$

In water, the solution of Rayleigh equation is fairly simple since there is no basic flow: $\hat{\psi}_a(z) = -ac\, e^{-kz}$. Nevertheless, this eigenvalue problem is still analytically very hard to solve. Young and Wolfe [27] made it for a double exponential profile. Otherwise, it has been numerically solved by Morland and Saffman [28]. But since the coupling between wind and waves is small due to the natural small parameter $\epsilon = \frac{\rho_a}{\rho_w}$, Miles could solve it perturbatively with the expansions

$$c = c_0 + \epsilon c_1 + \epsilon^2 c_2 + \ldots \qquad \text{and} \qquad \hat{\psi} = \hat{\psi}_0 + \epsilon\hat{\psi}_1 + \epsilon^2\hat{\psi}_2 + \ldots, \qquad \epsilon \ll 1. \tag{2.37}$$

with $c_0 = \sqrt{\frac{g}{k}}$. He eventually obtained the following expression for the growth rate:

$$\gamma = -\pi\epsilon c_0 \frac{U_{zz}(z_c)}{|U_z(z_c)|}|\chi(z_c)|^2, \qquad \text{where} \qquad U(z_c) = c_0 \tag{2.38}$$

defines a critical layer (see figure 2.3) and $\chi = \frac{\hat{w}}{\hat{w}(0)}$ is solution of

$$(U-c_0)(\chi_{zz} - k^2\chi) - U_{zz}\,\chi = 0, \qquad \chi(0) = 1, \qquad \chi(z) \underset{+\infty}{\propto} e^{-kz}. \tag{2.39}$$

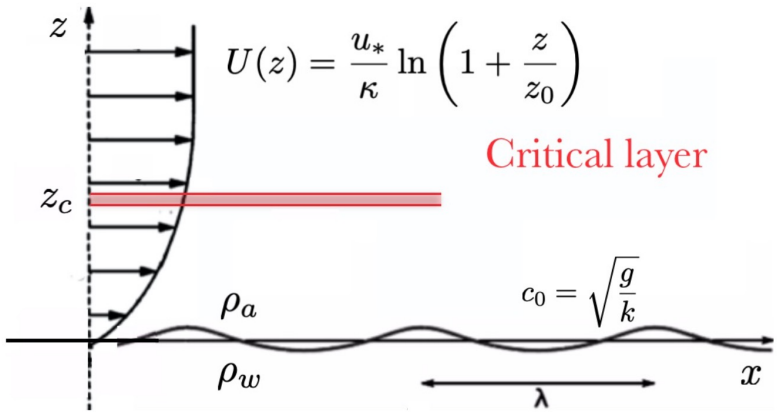

Figure 2.3: Schematic of a critical layer, defined as the level where the wind velocity matches the phase speed of the wave.

Chapter 3

A numerical and asymptotic study of the growth rate of wind waves

We present in this chapter our research's results.

3.1 Mathematical statement of the problem

In this section, the dimensional variables are denoted with a star.

Let us consider a deep water gravity wave with wavenumber k_* on the water surface, over which blows a wind represented by the profile $U_*(z_*)$. The calculation of the growth rate given by Miles' formula (2.38) involves the solution of

$$\chi''(z_*) = \left\{ k_*^2 + \frac{U_*''(z_*)}{U_*(z_*) - \sqrt{\frac{g}{k_*}}} \right\} \chi(z_*), \qquad \chi(0) = 1, \qquad \chi(z_*) \underset{+\infty}{\propto} e^{-k_* z_*}. \tag{3.1}$$

Let U_0 be the characteristic velocity of the wind and L a characteristic vertical length scale. Dimensionless variables are then defined as follows:

$$k = k_* L, \qquad U = \frac{U_*}{U_0}, \qquad z = \frac{z_*}{L}. \tag{3.2}$$

Hence, the dimensionless form of (3.1) is

$$\chi''(z) = \left\{ k^2 + \frac{U''(z)}{U(z) - \frac{1}{Fr\sqrt{k}}} \right\} \chi(z), \qquad \chi(0) = 1, \qquad \chi(z) \underset{+\infty}{\propto} e^{-kz}. \tag{3.3}$$

We have introduced the Froude number $Fr = \frac{U_0}{\sqrt{gL}}$ whose denominator is the phase velocity of gravity mode of wave length L. In hydraulics, this number characterizes the flow in a canal where L corresponds to its depth: it is said subcritical when $Fr < 1$ and supercritical when $Fr > 1$. We could keep those denominations for the wind.

We denote $c = \frac{1}{Fr\sqrt{k}}$ the dimensionless phase velocity of surface gravity waves. k is the ratio of the vertical and horizontal length scales, so $k \gg 1$ and $k \ll 1$ correspond to short and long waves respectively.

We require the following properties for the wind profile:

1. $U(0) = 0$ due to the no-slip condition at the water surface.
2. $U' > 0$ so that there is only one critical layer.
3. $U'' < 0$ to ensure the growth of waves.

4. $\lim_{z\to+\infty} U''(z) = 0$ for the desired asymptotic behaviour of χ to make sense.

We will mostly focus on the standard profiles $U_1(z) = 1-e^{-z}$ and $U_2(z) = \ln(1+z)$. Note that the exponential profile is bounded, so L is the thickness of the air boundary layer in that case. As a consequence, it restricts the range of values of k and Fr which have to be such that $c < 1$. The logarithmic profile is more relevant from a physics perspective because it comes from the theory of turbulent boundary layers; L is then interpreted as the roughness of the waves.

The exact analytical solution of the boundary value problem (3.3) for an arbitrary wind profile is out of reach. In section 3.2, we develop an efficient scheme for solving it numerically, then compute the growth rate and compare it with experimental data; meanwhile, we show that our scheme is applicable to a wide class of problems. In section 3.3, we derive asymptotic solutions of (3.3) in the short and long wave approximations.

3.2 Numerics

In 1959, Conte and Miles [29] developed an algorithm based on the Frobenius' series to compute the coefficient β but it works only for the logarithmic profile. Almost fifty years later, Beji and Nadaoka [30] proposed a method for solving (3.3) for an arbitrary wind profile. We considerably improved its efficiency by separating the integration of real and imaginary parts and defining a simpler criterion of convergence at infinity. Moreover, we noticed that their sophisticated local solutions can be readily replaced by the leading order terms of the Frobenius' series. This way, we obtained a general procedure for solving linear boundary value problems having one or more regular singularities. Accuracy of our scheme has been checked by recovering the results of [29]. We realized during the writing of this work that ten years after the publication of [29], Hughes and Reid [31] had developed a scheme based on the same ideas, though with a different treatment at infinity, in their study of the exponential profile which is not cited in [30].

In this section, we first summarize the results on the Frobenius' series for this problem. Then, we refine the local analysis of [30] and detail our improvement of their numerical method. We eventually expose the generalization of the scheme.

3.2.1 Frobenius' series

There is a singularity at $z = z_c$, defined as $U(z_c) = c$, that makes the resolution of (3.3) challenging. Let us expand U in a Taylor series about z_c, denoting the derivatives at this point with a subscript c :

$$U(z) = \sum_{n=0}^{+\infty} U_c^{(n)} \frac{(z-z_c)^n}{n!}, \tag{3.4}$$

$$U''(z) = \sum_{n=2}^{+\infty} U_c^{(n)} \frac{(z-z_c)^{n-2}}{(n-2)!}, \tag{3.5}$$

$$\frac{U''(z)}{U(z)-c} = \frac{\sum_{n=0}^{+\infty} U_c^{(n+2)} \frac{(z-z_c)^n}{n!}}{\sum_{n=1}^{+\infty} U_c^{(n)} \frac{(z-z_c)^n}{n!}} \underset{z_c}{\sim} \frac{U_c''}{U_c'(z-z_c)}. \tag{3.6}$$

We assume that both U_c' and U_c'' are non-zero. Therefore, the singularity at $z = z_c$ is regular and we can look for solutions of the form [32]

$$\chi(z) = \sum_{j=0}^{+\infty} a_j (z-z_c)^{j+s}, \quad \text{with } a_0 \neq 0. \tag{3.7}$$

Using the expansions (3.4) and (3.5), we find the indicial exponents $s_1 = 1$ and $s_2 = 0$, differing by an integer. Thus, two linearly independent solutions of the Rayleigh equation are

$$\chi_1(z) = \sum_{j=0}^{+\infty} a_j (z-z_c)^{j+1}, \tag{3.8}$$

$$\chi_2(z) = \sum_{j=0}^{+\infty} b_j (z-z_c)^j + C\ \chi_1(z)\ \mathrm{Log}(z-z_c), \tag{3.9}$$

where

$$\mathrm{Log}(z-z_c)=\begin{cases}\ln(z-z_c) & \text{if } z>z_c\\ \ln|z-z_c|+i\pi & \text{if } z<z_c\end{cases} \tag{3.10}$$

denotes the principal determination of the complex logarithm, with a branch cut just below the negative real axis. According to Fuchs' theorem, those series are converging. As usual, we set $a_0=1$ and $b_0=1$; the coefficient $b_{s_1-s_2}=b_1$ is undetermined, so we can choose $b_1=0$. After some algebra, we find $a_1=\frac{U_c''}{2U_c'}$ and $C=\frac{U_c''}{U_c'}$. Furthermore, for $n\geqslant 2$ and $\forall(j,m)\in\mathbb{N}\times\mathbb{N}^\star$,

$$\sum_{\substack{(m,j)/\\ n=m+j+1}}\left[(j+2)(j+3)\frac{U_c^{(m)}}{m!}a_{j+2}-\frac{U_c^{(m+1)}}{(m-1)!}a_{j+1}-k^2\frac{U_c^{(m)}}{m!}a_j\right]=\frac{U_c^{(n+1)}}{(n-1)!}-\frac{U_c''}{U_c'}\frac{U_c^{(n)}}{n!}, \tag{3.11}$$

$$\sum_{\substack{(m,j)/\\ n=m+j+1}}\left[(j+1)(j+2)\frac{U_c^{(m)}}{m!}b_{j+2}-\frac{U_c^{(m+1)}}{(m-1)!}b_{j+1}-k^2\frac{U_c^{(m)}}{m!}b_j+(2j+3)\frac{U_c''}{U_c'}\frac{U_c^{(m)}}{m!}a_{j+1}\right]=\frac{U_c^{(n+1)}}{(n-1)!}-\frac{U_c''}{U_c'}\frac{U_c^{(n)}}{n!}.$$

Thanks to these recursion relations, we are able to calculate one by one all coefficients a_j and b_j. The first terms are

$$\chi_1(z)=z-z_c+\frac{U_c''}{2U_c'}(z-z_c)^2+\frac{1}{6}\left(k^2+\frac{U_c'''}{U_c'}\right)(z-z_c)^3+\mathcal{O}(z-z_c)^4, \tag{3.12}$$

$$\chi_2(z)=\frac{U_c''}{U_c'}\,\chi_{k,1}(z)\,\mathrm{Log}(z-z_c)+1+\left[\frac{k^2}{2}+\frac{U_c'''}{2U_c'}-\left(\frac{U_c''}{U_c'}\right)^2\right](z-z_c)^2+\mathcal{O}(z-z_c)^3. \tag{3.13}$$

They are the so-called Tollmien inviscid solutions [25], in terms of which the boundary value problem (3.3) can be theoretically solved:

$$\chi(z)=A_1\,\chi_1(z)+A_2\,\chi_2(z),\qquad (A_1,A_2)\in\mathbb{C}^2. \tag{3.14}$$

However in practice, the calculation of the coefficients A_1 and A_2 is a very difficult task. We readily notice that $\chi(z_c)=A_2$ and that all derivatives diverge at z_c.

3.2.2 A local (modified) Bessel equation

Following [30], in order to study the behaviour of the solutions of the Rayleigh equation around the singularity, we keep only the first term in the Taylor series (3.4) and (3.5):

$$\chi''(z)=\left(k^2+\frac{U_c''}{U_c'(z-z_c)}\right)\chi(z). \tag{3.15}$$

$(z-z_c)^{-1}$ becomes very large near z_c so that we can discard the term proportional to k^2. Moreover, we perform the change of variable $\mathfrak{z}=-\frac{U_c''}{U_c'}\,(z-z_c)$ and obtain

$$\mathfrak{z}\,\mathcal{X}''(\mathfrak{z})+\mathcal{X}(\mathfrak{z})=0. \tag{3.16}$$

This ODE looks very simple, however the coefficient of the second derivative can change sign so that we expect a different behaviour on each side of the singularity. Performing the transformation

$$\mathcal{X}(\mathfrak{z})=\begin{cases}\frac{\xi}{2}\,\Psi^+(\xi),\ \xi=2\sqrt{\mathfrak{z}} & \text{if } \mathfrak{z}>0\\ \frac{\xi}{2}\,\Psi^-(\xi),\ \xi=2\sqrt{-\mathfrak{z}} & \text{if } \mathfrak{z}<0\end{cases}, \tag{3.17}$$

it is mapped to a Bessel equation above the singularity and a modified Bessel equation below:

$$\xi^2\,\frac{d^2\Psi^+}{d\xi^2}+\xi\,\frac{d\Psi^+}{d\xi}+(\xi^2-1)\,\Psi^+(\xi)=0, \tag{3.18}$$

$$\xi^2\,\frac{d^2\Psi^-}{d\xi^2}+\xi\,\frac{d\Psi^-}{d\xi}-(\xi^2+1)\,\Psi^-(\xi)=0. \tag{3.19}$$

Hence, the general solution of equation (3.16) is

$$\mathcal{X}(\mathfrak{z}) = \begin{cases} \sqrt{\mathfrak{z}}\left[A\, J_1(2\sqrt{\mathfrak{z}}) + B\, Y_1(2\sqrt{\mathfrak{z}})\right] & \text{if } \mathfrak{z} > 0 \\ \sqrt{-\mathfrak{z}}\left[C\, I_1(2\sqrt{-\mathfrak{z}}) + D\, K_1(2\sqrt{-\mathfrak{z}})\right] & \text{if } \mathfrak{z} < 0 \end{cases}, \tag{3.20}$$

where A, B, C, D are complex constants. However, they are not independent because the two expressions in (3.20) should have the same analytic continuation on their Riemann surface. In addition, $\mathcal{X}$ should be continuous at the singularity since both Frobenius' exponents are positive. For $\mathfrak{z} \leqslant 0$, $\sqrt{\mathfrak{z}} = \pm i\sqrt{-\mathfrak{z}}$ is multivalued because of the algebraic branch point $\mathfrak{z} = 0$. We choose to work on the principal sheet, defined by the polar angle $\theta \in]-\pi, \pi]$. In so doing, we select $+$ and then invoke the functional relations

$$\forall x > 0, \quad J_1(ix) = i\, I_1(x) \quad \text{and} \quad Y_1(ix) = \frac{2i}{\pi}\, K_1(x) - I_1(x). \tag{3.21}$$

Note that the origin is a concomitant logarithmic branch point due to the (modified) Bessel functions of second kind. One can match the two expressions of χ given in (3.20) and get the conditions

$$\begin{cases} C = -(A + iB) \\ D = -\frac{2B}{\pi} \end{cases}, \tag{3.22}$$

which are dependent on our choice of Riemann's sheet.

The advantage of the form of the solution (3.20) is that it is a linear combination of real functions on each interval. Therefore, we can conveniently split real and imaginary parts, which will be very helpful for the numerical integration. Since $J_1(0) = 0$ and $Y_1(x) \underset{0}{\sim} -\frac{2}{\pi x}$, we readily find $\chi_k(z_c) = -\frac{B}{\pi}$.

3.2.3 Improvement of Beji and Nadaoka's method

For the sake of convenience, let us introduce some notations:

$$\mathcal{X}_1(\mathfrak{z}) = \sqrt{\mathfrak{z}}\, J_1(2\sqrt{\mathfrak{z}}), \qquad \mathcal{X}_2(\mathfrak{z}) = \sqrt{\mathfrak{z}}\, Y_1(2\sqrt{\mathfrak{z}}), \tag{3.23}$$

$$\mathcal{X}_3(\mathfrak{z}) = \sqrt{-\mathfrak{z}}\, I_1(2\sqrt{-\mathfrak{z}}), \qquad \mathcal{X}_4(\mathfrak{z}) = \sqrt{-\mathfrak{z}}\, K_1(2\sqrt{-\mathfrak{z}}). \tag{3.24}$$

With $A = a + ib$ and $B = c + id$, the real and imaginary parts of the solution (3.20) are

$$\Re\{\mathcal{X}^+\} = a\, \mathcal{X}_1 + c\, \mathcal{X}_2, \tag{3.25}$$

$$\Im\{\mathcal{X}^+\} = b\, \mathcal{X}_1 + d\, \mathcal{X}_2, \tag{3.26}$$

$$\Re\{\mathcal{X}^-\} = (d - a)\, \mathcal{X}_3 - \frac{2c}{\pi}\, \mathcal{X}_4, \tag{3.27}$$

$$\Im\{\mathcal{X}^-\} = -(b + c)\, \mathcal{X}_3 - \frac{2d}{\pi}\, \mathcal{X}_4. \tag{3.28}$$

Let us rewrite the boundary conditions in (3.3) as well:

$$\begin{cases} \Re\{\chi\}(0) = 1 \\ \Im\{\chi\}(0) = 0 \\ \Re\{\chi'\}(z) + k\, \Re\{\chi\}(z) \underset{+\infty}{\to} 0 \\ \Im\{\chi'\}(z) + k\, \Im\{\chi\}(z) \underset{+\infty}{\to} 0 \end{cases}. \tag{3.29}$$

We insist on the fact that the solutions (3.25) to (3.28) are not valid where those boundary conditions apply. Thus, we are going to develop a variant of a shooting method. The idea is to use our local solutions to generate initial conditions near the singularity and numerically integrate the Rayleigh equation up and down until "infinity" (to be specified) and zero respectively. Let us denote $r = -\frac{U_c''}{U_c'} > 0$ and make a jump of amplitude $\delta = 10^{-6}$ on each side of the singularity. Basically, $\mathcal{X}^+(r\delta)$ and $\mathcal{X}^-(-r\delta)$ serve as initial conditions for the numerical integration and we have to find the proper coefficients a, b, c, d so that the boundary conditions (3.29) are satisfied.

So as to integrate the Rayleigh equation, we express it as a 2-dimensional first order ODE:

$$\boldsymbol{u}' = \mathcal{A}\boldsymbol{u}, \quad \text{with} \quad \boldsymbol{u} = \begin{pmatrix} \chi \\ \chi' \end{pmatrix} \quad \text{and} \quad \mathcal{A}(z) = \begin{pmatrix} 0 & 1 \\ k^2 + \frac{U''(z)}{U(z)-c)} & 0 \end{pmatrix}. \tag{3.30}$$

Then, for an initial condition $\boldsymbol{u_0}$ at z_0 a formal solution of that equation is

$$\boldsymbol{u}(z) = \mathcal{L}(z, z_0)\, \boldsymbol{u_0}, \qquad \text{with} \qquad \mathcal{L}(z, z_0) \equiv \mathcal{T} e^{\int_{z_0}^{z} \mathcal{A}(z')dz'}. \tag{3.31}$$

$\mathcal{T}$ is the time ordering operator. Defining $\boldsymbol{u_j} \triangleq (\mathcal{X}_j, \mathcal{X}_j')^t \ \forall j \in [\![1, 4]\!]$, the local solutions (3.25) to (3.28) yield a set of initial conditions at $z_c \pm \delta$:

$$\boldsymbol{u_r^+} = a\, \boldsymbol{u_1}(r\delta) + c\, \boldsymbol{u_2}(r\delta), \tag{3.32}$$

$$\boldsymbol{u_i^+} = b\, \boldsymbol{u_1}(r\delta) + d\, \boldsymbol{u_2}(r\delta), \tag{3.33}$$

$$\boldsymbol{u_r^-} = (d-a)\, \boldsymbol{u_3}(-r\delta) - \frac{2c}{\pi}\, \boldsymbol{u_4}(-r\delta), \tag{3.34}$$

$$\boldsymbol{u_i^-} = -(b+c)\, \boldsymbol{u_3}(-r\delta) - \frac{2d}{\pi}\, \boldsymbol{u_4}(-r\delta). \tag{3.35}$$

At this stage, we use the essential fact that $\mathcal{L}(z, z_0)$ is a linear operator.

$$\Re\{\boldsymbol{u}(z)\} = \begin{cases} \mathcal{L}(z, z_c+\delta)\, \boldsymbol{u_r^+} = a\, \mathcal{L}(z, z_c+\delta)\, \boldsymbol{u_1}(r\delta) + c\, \mathcal{L}(z, z_c+\delta)\, \boldsymbol{u_2}(r\delta) & \text{if } z > z_c \\ \mathcal{L}(z, z_c-\delta)\, \boldsymbol{u_r^-} = (d-a)\, \mathcal{L}(z, z_c-\delta)\, \boldsymbol{u_3}(-r\delta) - \frac{2c}{\pi}\, \mathcal{L}(z, z_c-\delta)\, \boldsymbol{u_4}(-r\delta) & \text{if } z < z_c \end{cases},$$

$$\Im\{\boldsymbol{u}(z)\} = \begin{cases} \mathcal{L}(z, z_c+\delta)\, \boldsymbol{u_i^+} = b\, \mathcal{L}(z, z_c+\delta)\, \boldsymbol{u_1}(r\delta) + d\, \mathcal{L}(z, z_c+\delta)\, \boldsymbol{u_2}(r\delta) & \text{if } z > z_c \\ \mathcal{L}(z, z_c-\delta)\, \boldsymbol{u_i^-} = -(b+c)\, \mathcal{L}(z, z_c-\delta)\, \boldsymbol{u_3}(-r\delta) - \frac{2d}{\pi}\, \mathcal{L}(z, z_c-\delta)\, \boldsymbol{u_4}(-r\delta) & \text{if } z < z_c \end{cases}.$$

Now, $\mathcal{L}(z, z_c \pm \delta)\, \boldsymbol{u_j}(\pm r\delta) \equiv \big(\chi_j(z), \chi_j'(z)\big)^t$ is nothing but the solution of equation (3.30) at $z \gtrless z_c$ satisfying the initial condition $\boldsymbol{u_j}(\pm r\delta)$ at $z_c \pm \delta$. We are clearly not able to analytically calculate the time ordered exponential operator but we can numerically compute this solution for any z. We define the upper limit of integration as $z_\infty = -\frac{1}{k}\ln(\chi_{min})$ with for instance $\chi_{min} = 10^{-3}$. The boundary conditions (3.29) are eventually reduced to the simple algebraic system

$$\begin{pmatrix} -\chi_3(0) & 0 & -\frac{2}{\pi}\chi_4(0) & \chi_3(0) \\ 0 & -\chi_3(0) & -\chi_3(0) & -\frac{2}{\pi}\chi_4(0) \\ \chi_1'(z_\infty) + k\,\chi_1(z_\infty) & 0 & \chi_2'(z_\infty) + k\,\chi_2(z_\infty) & 0 \\ 0 & \chi_1'(z_\infty) + k\,\chi_1(z_\infty) & 0 & \chi_2'(z_\infty) + k\,\chi_2(z_\infty) \end{pmatrix} \begin{pmatrix} a \\ b \\ c \\ d \end{pmatrix} = \begin{pmatrix} 1 \\ 0 \\ 0 \\ 0 \end{pmatrix},$$

which can be solved analytically. The trick we have used in the above derivation can be formally stated as follows:

Lemma 1. *Let (E) be a n-dimensional linear first order ODE on a field $\mathbb{K}$, whose independant variable will be denoted t. Let $\boldsymbol{\alpha}, \boldsymbol{\beta} \in \mathbb{K}^n$. If $\boldsymbol{f_\alpha}$ and $\boldsymbol{f_\beta}$ are solutions of (E) satisfying the initial conditions $(t_0, \boldsymbol{\alpha})$ and $(t_0, \boldsymbol{\beta})$ respectively, then $\lambda\, \boldsymbol{f_\alpha} + \mu\, \boldsymbol{f_\beta}$ is the solution of (E) satisfying the initial condition $(t_0, \lambda\, \boldsymbol{\alpha} + \mu\, \boldsymbol{\beta})$ for any λ and μ in $\mathbb{K}$.*

This numerical scheme depends on which Riemann's sheet we choose to work on, through the relations (3.22). For example, if we instead opt for the sheet defined by the polar angle $\theta \in]-3\pi, -\pi]$, then for $\mathfrak{z} \leqslant 0$, $\sqrt{\mathfrak{z}} = -i\sqrt{-\mathfrak{z}}$ and we now shall use

$$\forall x > 0, \quad J_1(-ix) = -i\, I_1(x) \quad \text{and} \quad Y_1(-ix) = -\frac{2i}{\pi}\, K_1(x) - I_1(x). \tag{3.36}$$

It yields $C = -(A - iB)$ and $D = -\frac{2B}{\pi}$. Nonetheless, one can check that it leads to the complex conjugate of the present solution. This is fine because we are interested only in its modulus.

3.2.4 General Frobenius-based scheme for linear singular boundary value problems

The local solutions we have used in the previous section come from an analysis specific to the Rayleigh equation. Nonetheless, the leading order terms of the Tollmien inviscid solutions (3.12) and (3.13) provide us another set of local solutions:

$$\chi_{loc}(z) = A_1(z - z_c) + A_2\left\{1 + \frac{U_c''}{U_c'}(z - z_c)\,\mathrm{Log}(z - z_c)\right\}. \tag{3.37}$$

There is no need to include more terms in the expansion because this local solution will be evaluated extremely close to the singularity ($z - z_c = 10^{-6}$). In fact, if we Taylor-expand (3.20) about $\mathfrak{z} = 0$ we get back (3.37); that makes sense since one way of defining the (modified) Bessel functions is by their Frobenius' series.

Now, we can repeat the procedure we have just described. With $A_1 = a_1 + ib_1$ and $A_2 = a_2 + ib_2$, we find

$$\Re\{\chi_{loc}^+\} = a_1\,\chi_{loc,1} + a_2\,\chi_{loc,2}, \tag{3.38}$$

$$\Im\{\chi_{loc}^+\} = b_1\,\chi_{loc,1} + b_2\,\chi_{loc,2}, \tag{3.39}$$

$$\Re\{\chi_{loc}^-\} = \left(a_1 - \pi b_2\frac{U_c''}{U_c'}\right)\chi_{loc,1} + a_2\,\chi_{loc,2}, \tag{3.40}$$

$$\Im\{\chi_{loc}^-\} = \left(b_1 + \pi a_2\frac{U_c''}{U_c'}\right)\chi_{loc,1} + b_2\,\chi_{loc,2}, \tag{3.41}$$

where $\chi_{loc,1}(z) = z - z_c$ and $\chi_{loc,2}(z) = 1 + \frac{U_c''}{U_c'}(z - z_c)\ln|z - z_c|$. After integration from $z_c \pm \delta$ and application of the boundary conditions (3.29), we get another algebraic system for the coefficients a_1, a_2, b_1, b_2 whose analytical solution is also known.

Note that if we had taken the branch cut just above the negative real axis (instead of below), then we would have got $-i\pi$ in the complex logarithm (3.10), which impacts (3.37). But from the analytical expression of the coefficients a_1, a_2, b_1, b_2 in terms the integrated local solutions, we can show that the transformation $\pi \to -\pi$ implies $a_1 \to a_1$, $a_2 \to a_2$, $b_1 \to -b_1$ and $b_2 \to -b_2$. We conclude that moving the branch cut from the lower to the upper part of the complex plane is equivalent to take the complex conjugate of the solution. This is the counterpart of our discussion about Riemann's sheets in the end of the previous section. The reason for such a phenomenon is that when integrating a function with a singularity on the real axis, one has to make a detour either in upper or the lower part of the complex plane.

Since the Frobenius' series always exists for linear ODEs and are converging about any regular singular point, our scheme could be used to solve other problems. The most general one we can think of is of the form $\boldsymbol{y}' = \mathcal{A}\boldsymbol{y}$ together with n boundary conditions, and $\mathcal{A}$ a n-dimensional complex matrix function on $\mathbb{R}$ having one or several regular singularities. In addition, if some boundary conditions are at infinity, the corresponding asymptotic behaviour of the solution should be known so that one can define the limits of integration, as we did for z_∞. We propose to deal with the case of two (or more) singularities as follows. One has got a linear combination of n local solutions around each singularity. There is no reason for the coefficients of those linear combinations to be the same. Thus, one is left with $2n$ coefficients to compute but still only n boundary conditions. One shall choose n points between the singularities and impose the integrated linear combinations to be equal at these points. Note however that in dimension $n > 2$, the question of well-posedness of the problem should be addressed before any numerical attempt to solve it.

3.2.5 Comparison of Miles' theory with Plant's experimental data

In 1982, Plant gathered four data sets of measurements of initial growth rates [33]. He plotted the growth rate normalized by the frequency, which represents the strength of wind-wave interaction, as a function of the wind-forcing of waves $\frac{u_\star}{c}$. Thanks to our numerical scheme, we compute the growth rate given by Miles' formula (2.38) and confront it to this experimental data in figure 3.1 with $Fr = \frac{u_\star}{\kappa\sqrt{g z_0}} = 18.25$. There is a pretty good agreement for $\frac{u_\star}{c} < 2$, although the data points are pretty scattered. Note that Mitsuyasu and Honda [34] produced the same year as Plant a similar figure with their own experimental data, unfortunately as scattered as his. There is an ongoing work together with the asymptotics developed in section 3.3 to understand the discrepancy between Miles' theory and experiments for $\frac{u_\star}{c} > 2$. In addition, we seek to rationalize the power law that seems to appear in figure 3.1.

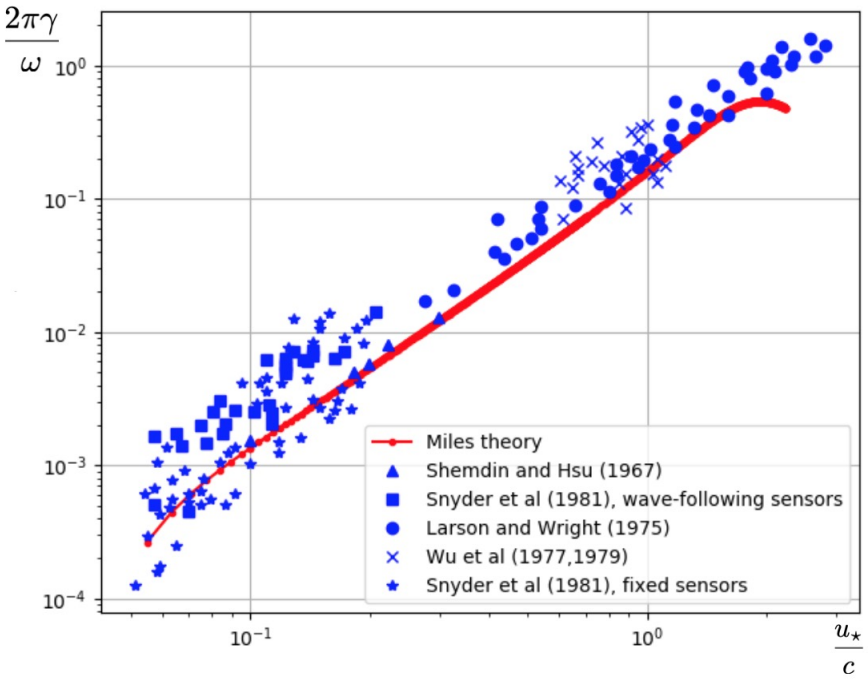

Figure 3.1: Comparison of Miles' theory with Plant's experimental data.

3.3 Asymptotics

An exact analytical solution of the Rayleigh equation in terms of hypergeometric functions was obtained for the exponential profile by Hughes and Reid in their paper [31] published in 1965. It was then used by Miles himself to solve the boundary-value problem (3.3) for this profile, in the appendix of a paper by Morland and Saffman published in 1993 [28]. Moreover, since hypergeometric functions provide very little intuition of the actual behaviour of the solution, he also calculated approximate expressions for small and large wavenumbers. The same year, when he revisited his theory, Miles included other effects from turbulence and proposed an approximate formula his growth rate [35]. In this section, we also study long and short waves but working directly on Rayleigh equation in order to draw general asymptotic features for a wind profile having the minimal properties given in section 3.1.

3.3.1 Short waves

Let us consider short waves, which means that $k \gg 1$. Therefore, we can introduce the small parameter $\epsilon = \frac{1}{k}$ and get to solve

$$\epsilon^2 \chi''(z) = \left\{ 1 + \epsilon^2 \frac{U''(z)}{U(z) - \frac{\sqrt{\epsilon}}{Fr}} \right\} \chi(z), \qquad \chi(0) = 1, \qquad \lim_{z \to +\infty} \chi(z) = 0. \tag{3.42}$$

The Froude number affects only the position of the singularity. Since U is monotonic, we can define its inverse function U^{-1} which has the same monotonicity. Then $z_c = U^{-1}\left(\frac{\sqrt{\epsilon}}{Fr}\right)$ and so for a fixed ϵ, the smaller Fr the larger z_c.

The small parameter multiplies the highest derivative so we shall perform a singular perturbation analysis. However, this equation does not have a form appearing in the standard textbooks on asymptotic methods ; it is a Schrödinger-like equation whose potential depends on the small parameter. Thus, the WKB method is not applicable. We are going to use instead the boundary layer theory. We indeed expect a boundary layer at the singularity, since the second derivative becomes infinite at this point, but its structure should not be the same for the real and the imaginary parts because they satisfy different boundary conditions. Note that the position of this internal boundary depends on the small parameter, in addition to Fr, which is unusual.

We seek an outer solution in the form of a perturbation series in power of ϵ:

$$\chi_{out}(z) = \chi_0(z) + \epsilon\chi_1(z) + \epsilon^2\chi_2(z) + \dots, \qquad \epsilon \to 0_+, \tag{3.43}$$

which immediately leads to $\chi_0 = 0$. In words, the outer solution at leading order is identically zero.

Let us define an inner variable $Z = \frac{z-z_c}{\delta}$, where $\delta > 0$ is the thickness of the boundary layer, and an inner solution $X_{in}(Z)$. To determine $\delta(\epsilon)$, we rewrite the local equation (3.15) in terms of the new variable and look for a dominant balance:

$$\left(\frac{\epsilon}{\delta}\right)^2 X_{in}''(Z) = \left\{1 + \frac{\epsilon^2}{\delta}\frac{U_c''}{U_c' Z}\right\} X_{in}(Z), \qquad Z = \mathcal{O}(1). \tag{3.44}$$

The ratio $\frac{U_c''}{U_c'}$ a priori depends on ϵ because z_c does. Nonetheless, for physically relevant profiles $\left|\frac{U_c''}{U_c'}\right| \leqslant 1$ so that we readily get the distinguished limit $\delta = \epsilon$. The appropriate perturbation expansion of the inner solution is

$$X_{in}(Z) = X_0(Z) + \epsilon X_1(Z) + \epsilon^2 X_2(z) + \dots, \quad \epsilon \to 0_+, \tag{3.45}$$

which leads to

$$X_0''(Z) = X_0(Z). \tag{3.46}$$

The general solution of this ODE is $X_0(Z) = C_1\, e^{-Z} + C_2\, e^{Z}$ with $(C_1, C_2) \in \mathbb{C}^2$. Very unexpectedly, the inner solution at leading order has no singularity.

Now that the thickness of the boundary layer is known, we come back on the key fact that its position depends on ϵ and Fr. If $z_c = \mathcal{O}(\epsilon)$ or even $z_c \ll \epsilon$, then the boundary layer actually touches the lower boundary. Subsequently, there is only one outer region. We first accomplish the matching between inner and outer solutions in this case. The constants C_1 and C_2 are determined by the matching principle

$$\lim_{z \to z_{c+}} \chi_0(z) = \lim_{Z \to +\infty} X_0(Z). \tag{3.47}$$

To preclude divergence, we have to choose $C_2 = 0$. We are in the case where the inner solution is in fact valid at $z = 0$, so C_1 is found by enforcing the boundary condition at this point:

$$X_0\left(-\frac{z_c}{\epsilon}\right) = 1 \qquad \Rightarrow \qquad C_1 = e^{-\frac{z_c}{\epsilon}}. \tag{3.48}$$

Hence, $X_0(Z) = e^{-Z-\frac{z_c}{\epsilon}}$. A composite solution is constructed using the additive rule of Van Dyke, hence

$$\chi_{unif,0}(z) = \text{inner} + \text{outer} - \text{common part} = e^{-\frac{z}{\epsilon}}. \tag{3.49}$$

Finally, let us deal with the case where $z_c \gg \epsilon$ meaning there is an outer region between the lower boundary and the critical layer. Note that for a given ϵ, it is the value of the Froude number which makes the distinction between the two cases. Basically, this one occurs when $Fr < 1$ and the previous one when $Fr > 1$. The solution at leading order is the same in both outer regions, so we still have $C_2 = 0$. And from the matching principle

$$\lim_{z \to z_{c-}} \chi_0(z) = \lim_{Z \to -\infty} X_0(Z), \tag{3.50}$$

we infer $C_2 = 0$. However the calculation is not over. Indeed, the imaginary part of χ_0 trivially obeys the boundary condition at $z = 0$ but its real part does not. Thus, the real part of the solution at leading order must have another boundary layer at $z = 0$. Let us examine its structure: it is standard to regard the coefficients of a linear ODE as constant within a boundary layer. Since $U(0) = 0$, we get

$$\epsilon^2\, \chi''(z) = \left\{1 - \epsilon^{\frac{3}{2}}\, Fr\, U''(0)\right\} \chi(z), \qquad \text{around } z = 0. \tag{3.51}$$

We are in the case where $Fr < 1$ and $U''(0) = \mathcal{O}(1)$ for physically relevant profiles. Then, one readily shows that this boundary layer also has a thickness ϵ. Defining a new inner variable $\mathcal{Z} = \frac{z}{\epsilon}$ and the corresponding inner solution $\mathfrak{X}_{in}(\mathcal{Z})$, the above equation becomes at leading order

$$\mathfrak{X}_0''(\mathcal{Z}) = \mathfrak{X}_0(\mathcal{Z}). \tag{3.52}$$

The solution in the internal boundary layer being identically zero, this is actually a situation identical to the case $Fr > 1$. Therefore, we infer $\mathfrak{X}_0(\mathcal{Z}) = e^{-\mathcal{Z}}$ and the same composite solution as previously.

We conclude that in the limit of large k and for any value of Fr, the leading order solution of the boundary value problem is real, equal to the free-stream solution e^{-kz}. This result is independent of the form of the wind profile. Furthermore, we have showed that it holds for any value of z_c, or equivalently, of $\frac{\sqrt{\epsilon}}{Fr}$. Hence, it is not affected by dispersion and is subsequently also valid for capillary waves. The comparison between the exact numerical solution obtained with our scheme and those general asymptotic results is very good even for $\epsilon = 0.1$, especially for large values of Fr; see figures 6.1 to 6.6 in the appendix.

3.3.2 Long waves

Let us consider long waves meaning that $k \ll 1$, that we can use a small parameter in (3.3). Still, we denote it ϵ to respect the tradition in asymptotics:

$$\chi''(z) = \left\{ \epsilon^2 + \frac{U''(z)}{U(z) - \frac{1}{Fr\sqrt{\epsilon}}} \right\} \chi(z), \qquad \chi(0) = 1, \qquad \lim_{z \to +\infty} \chi(z) = 0. \tag{3.53}$$

We are going to solve this problem with the method of matched asymptotic expansions. At first, we could be tempted to simply discard the term ϵ^2 however $\lim_{z \to +\infty} \frac{U''(z)}{U(z) - \frac{1}{Fr\sqrt{\epsilon}}} = 0_-$, so not only the term ϵ^2 is the dominant one for large z but, after the intermediate value theorem, there is a point $z_s > z_c$ where

$$\epsilon^2 + \frac{U''(z_s)}{U(z_s) - \frac{1}{Fr\sqrt{\epsilon}}} = 0. \tag{3.54}$$

The solution $\chi(z)$ has an inflexion point at $z = z_s$; its uniqueness can be ensured by requiring $U''' > 0$. We define a lower region $z \ll z_s$ and a higher region $z \gg z_s$, look for solutions within each of them and eventually match those solutions in the intermediate region around $z = z_s$. The equation to solve in the lower region is

$$\chi_L''(z) = \frac{U''(z)}{U(z) - \frac{1}{Fr\sqrt{\epsilon}}} \chi_L(z). \tag{3.55}$$

Let us study wether it is valid to extend the lower region until $z = 0$. Since $U(0) = 0$,

$$\left| \frac{U''(z)}{U(z) - \frac{1}{Fr\sqrt{\epsilon}}} \right| \underset{0}{\sim} Fr\sqrt{\epsilon}|U''(0)|. \tag{3.56}$$

For physically relevant profiles, $U''(0) = \mathcal{O}(1)$ so we can neglect the term ϵ^2 at the lower boundary provided that $Fr \gg \epsilon^{\frac{3}{2}}$. Then, denoting $c = \frac{1}{Fr\sqrt{\epsilon}}$, an obvious solution of equation (3.55) is $U - c$ from which one can readily construct another one, linearly independent. So the solutions in the lower region are

$$\chi_{L1}(z) = U(z) - c, \tag{3.57}$$

$$\chi_{L2}(z) = \chi_{L1}(z) \int^z \frac{dz'}{\chi_{L1}(z')^2}. \tag{3.58}$$

Up to now, we have been able to get solutions in the higher region only for the exponential profile U_1, that we expose below. We are currently seeking solutions for the logarithmic profile U_2 but its unbounded character makes it challenging. Unlike the solution in the short wave approximation, the one in the long wave approximation strongly depends on the form of the wind profile.

Solution for the profile U_1

For this profile, defined in section 3.1, it is very convenient to rewrite the problem in terms of the variable $\mathfrak{z} \equiv z - z_c$ introduced in section 3.2.2:

$$\mathcal{X}''(\mathfrak{z}) = \left\{ \epsilon^2 - \frac{e^{-\mathfrak{z}}}{1 - e^{-\mathfrak{z}}} \right\} \mathcal{X}(\mathfrak{z}), \qquad \mathcal{X}(-z_c) = 1, \qquad \lim_{z \to +\infty} \mathcal{X}(\mathfrak{z}) = 0. \tag{3.59}$$

The general solution in the lower region is $\mathcal{X}_L(\mathfrak{z}) = E\,\mathcal{X}_{L1}(\mathfrak{z}) + F\,\mathcal{X}_{L2}(\mathfrak{z})$, with $(E,F) \in \mathbb{C}^2$ and

$$\mathcal{X}_{L1}(\mathfrak{z}) = 1 - e^{-\mathfrak{z}}, \tag{3.60}$$

$$\mathcal{X}_{L2}(\mathfrak{z}) = \big(1 - e^{-\mathfrak{z}}\big)\left\{\frac{1}{1-e^{\mathfrak{z}}} + \mathrm{Log}\left(e^{\mathfrak{z}} - 1\right)\right\}. \tag{3.61}$$

In the higher region, the equation to solve is

$$\mathcal{X}''_H(\mathfrak{z}) = \big(\epsilon^2 - e^{-\mathfrak{z}}\big)\mathcal{X}_H(\mathfrak{z}), \qquad (G,H) \in \mathbb{C}^2. \tag{3.62}$$

which can be mapped to a Bessel equation of order 2ϵ by a smart change of variable. We infer its general solution:

$$\mathcal{X}_H(\mathfrak{z}) = G\,J_{2\epsilon}\big(2e^{-\frac{\mathfrak{z}}{2}}\big) + H\,J_{-2\epsilon}\big(2e^{-\frac{\mathfrak{z}}{2}}\big), \tag{3.63}$$

We have to take $H = 0$ for non-diverging solutions since $J_\nu(x) \underset{0}{\sim} \left(\frac{x}{2}\right)^\nu$. Note that we get the asymptotic exponential behaviour imposed in our numerical scheme. Since matching the two pieces of solution in the intermediate region is difficult, we try to connect them in a somewhat simpler manner. With the help of the numerics, we notice that there is an extremum in the intermediate region and choose to do patching at this point. We proceed as follows: we look for the position of the extremum in the higher region, then impose the solution in lower region to be extremal at this point and have the same value.

One can check that the equation $J'_{2\epsilon}\big(2e^{-\frac{\mathfrak{z}}{2}}\big) = 0$ has a unique solution on $\mathbb{R}_+$ for $\epsilon \ll 1$, which we denote $\mathfrak{z}_\star$. For the moment, this equation is solved numerically but we are also seeking possible approximate solutions.

By imposing $\mathcal{X}'_L(\mathfrak{z}_\star) = 0$, we get the relation

$$E + \left\{e^{\mathfrak{z}_\star} + 1 + \ln\left(e^{\mathfrak{z}_\star} - 1\right)\right\}F = 0. \tag{3.64}$$

Then the continuity of the solution at $z = \mathfrak{z}_\star$,

$$E\,\mathcal{X}_{L1}(\mathfrak{z}_\star) + F\,\mathcal{X}_{L2}(\mathfrak{z}_\star) = G\,J_{2\epsilon}\big(2e^{-\frac{\mathfrak{z}_\star}{2}}\big), \tag{3.65}$$

yields

$$E = e^{-\mathfrak{z}_\star} J_{2\epsilon}\big(2e^{-\frac{\mathfrak{z}_\star}{2}}\big)\left\{e^{\mathfrak{z}_\star} + 1 + \ln\left(e^{\mathfrak{z}_\star} - 1\right)\right\} G, \tag{3.66}$$

$$F = -e^{-\mathfrak{z}_\star} J_{2\epsilon}\big(2e^{-\frac{\mathfrak{z}_\star}{2}}\big)\, G. \tag{3.67}$$

Note that all these relations are independent of z_c, which appears only when we eventually impose the lower boundary condition:

$$\big(1 - e^{z_c}\big)\left[E + F\left\{\frac{1}{1-e^{-z_c}} + \ln\left(1 - e^{-z_c}\right) + i\pi\right\}\right] = 1. \tag{3.68}$$

After plugging (4.4) and (4.5) into it, we obtain the final expression

$$G = \frac{1}{e^{-\mathfrak{z}_\star} J_{2\epsilon}\big(2e^{-\frac{\mathfrak{z}_\star}{2}}\big)\big(1 - e^{z_c}\big)}\,\frac{K + i\pi}{K^2 + \pi^2}, \qquad K = e^{\mathfrak{z}_\star} + 1 - \frac{1}{1-e^{-z_c}} + \ln\left(\frac{e^{\mathfrak{z}_\star} - 1}{1 - e^{-z_c}}\right). \tag{3.69}$$

This calculation shows an excellent agreement with the numerical solution obtained with our scheme when $z_c = \mathcal{O}(1)$ or larger, even for $\epsilon = 0.1$. For small values of z_c, there is a discrepancy which can however be compensated by taking a tiny ϵ; see figures 6.7 to 6.11 in the appendix.

Chapter 4

Complementary information on waves in the ocean

In section 2.1, we have discarded several effects in the water wave problem so as to make the presentation of wave-wave interaction more accessible. We now show how to take them into account. In particular, we calculate the wave energy from which the ocean wave spectrum is defined in equation 1.1.

4.1 Water wave problem

We summarize here the water wave problem in its whole generality. It is a boundary value problem whose boundary conditions depend on the solution. We consider a 3-dimensional problem (2-dimensional waves) with the following notations: $\boldsymbol{r} = (x, y, z)^t$, $\boldsymbol{x} = (x, y)^t$ and $\boldsymbol{u} = \boldsymbol{u}^{\parallel} + w\, \boldsymbol{e}_z$.

We take a horizontal domain of finite extension $\mathcal{D} = \Delta x \times \Delta y$ with periodic boundary conditions. The projection of the gradient on $\mathcal{D}$ is denoted $\boldsymbol{\nabla}^{\parallel}$. We include both gravity and surface tension. In addition, the bottom topography is represented by a function $h(\boldsymbol{x})$.

We have to solve the Laplace equation $\nabla^2 \phi = 0$. The kinematic boundary conditions at the water surface and the uneven bottom are

$$\partial_t \eta + \boldsymbol{\nabla}^{\parallel} \phi \cdot \boldsymbol{\nabla}^{\parallel} \eta = \partial_z \phi \qquad \text{at} \qquad z = \eta(\boldsymbol{x}, t), \tag{4.1}$$

$$\partial_z \phi + \boldsymbol{\nabla}^{\parallel} \phi \cdot \boldsymbol{\nabla}^{\parallel} h = 0 \qquad \text{at} \qquad z = h(\boldsymbol{x}). \tag{4.2}$$

Furthermore, the dynamical boundary condition at the water surface is

$$\partial_t \phi + \frac{1}{2} \mid \boldsymbol{\nabla}\, \phi|^2 + g\eta + \frac{p}{\rho_w} = -\frac{\sigma}{\rho_w}\, \boldsymbol{\nabla}^{\parallel} \cdot \left(\frac{\boldsymbol{\nabla}^{\parallel} \eta}{\sqrt{1 + \mid \boldsymbol{\nabla}^{\parallel} \eta|^2}} \right) \qquad \text{at} \qquad z = \eta(\boldsymbol{x}, t). \tag{4.3}$$

4.2 Wave energetics

The wave energy is the mean energy per unit area: $E = T + V$ where T and V are the kinetic and potential energy parts respectively. Similarly, the wave momentum $\boldsymbol{M}$ is the mean momentum per unit area. Ocean waves are random so one has to use an ensemble averaging, which should obey Reynolds averaging rules. For random functions f, g and $a = cst$, they are the following [26]:

$$\langle f + g \rangle = \langle f \rangle + \langle g \rangle, \tag{4.4}$$

$$\langle af \rangle = a \langle f \rangle, \tag{4.5}$$

$$\langle a \rangle = a, \tag{4.6}$$

$$\langle \partial_s f \rangle = \partial_s \langle f \rangle \qquad \text{for} \qquad s = x, y, t, \tag{4.7}$$

$$\langle \langle f \rangle g \rangle = \langle f \rangle \langle g \rangle. \tag{4.8}$$

The combination of (4.6) and (4.8) leads to

$$\langle\langle f \rangle\rangle = \langle f \rangle . \tag{4.9}$$

In this section, we consider progressive periodic waves of small steepness so that results of the linear theory can be applied. Moreover, the averaging is then easy to define and can be related to the experimental point of view. Nonetheless, all results can be generalized to statistically homogeneous random wave fields provided that the water depth if constant. We assume it so; the kinematic boundary condition (4.2) is then reduced to

$$\partial_z \phi = 0 \qquad \text{at} \qquad z = 0. \tag{4.10}$$

Most of the results of this section can be found in the book by Phillips [36]. Nonetheless, our energetic interpretation of the ratio of group and phase velocities and its application making the calculation of the radiation stress tensor straightforward seems to be new.

4.2.1 Average definition(s) and reduction to a one-dimensional plane wave

Let us consider a surface displacement $\eta(\boldsymbol{x}, t)$ which has the form of a 2-dimensional progressive periodic wave. Then it is characterized by its period $\mathcal{T}$ together with its wavelengths L_x and L_y. Moreover, under some reasonable assumptions of regularity, it can be expanded in a Fourier series:

$$\eta(\boldsymbol{x}, t) = \sum_{n=1}^{+\infty} \Big\{ a_n \ \cos(n\ \boldsymbol{k} \cdot \boldsymbol{x} - \omega_n t) + b_n \ \sin(n\ \boldsymbol{k} \cdot \boldsymbol{x} - \omega_n t) \Big\}, \tag{4.11}$$

where $\boldsymbol{k} = \left(\frac{2\pi}{L_x}, \frac{2\pi}{L_y}\right)^t$, $\omega_1 = \frac{2\pi}{\mathcal{T}}$ and $\forall n \in \mathbb{N}^*,\ \omega_n = \omega(n\boldsymbol{k})$ with ω a function characterizing the dispersion.

$$a_n = \frac{4}{L_x L_y} \int_{-\frac{L_x}{2}}^{\frac{L_x}{2}} \int_{-\frac{L_y}{2}}^{\frac{L_y}{2}} \eta(\boldsymbol{x}, t=0) \cos(n\ \boldsymbol{k} \cdot \boldsymbol{x})\ dxdy, \tag{4.12}$$

$$b_n = \frac{4}{L_x L_y} \int_{-\frac{L_x}{2}}^{\frac{L_x}{2}} \int_{-\frac{L_y}{2}}^{\frac{L_y}{2}} \eta(\boldsymbol{x}, t=0) \sin(n\ \boldsymbol{k} \cdot \boldsymbol{x})\ dxdy. \tag{4.13}$$

It will be proved in section 4.2.5 that, in the absence of currents, the mean water level is equal to zero; reason why we took $a_0 = 0$.

We have adopted here the approach of Cauchy and Poisson to define the Fourier coefficients from the initial disturbance because the wavenumber spectrum is more convenient than the frequency spectrum for theoretical purposes. However, their definition with a time integration at an arbitrary point of $\mathcal{D}$ is also fine. In fact, in practice experimentalists take averages over one period. This operation trivially commutes with $\boldsymbol{\nabla}$ but does not with ∂_t. Conversely, an average over the wavelengths commutes with ∂_t but certainly not with $\boldsymbol{\nabla}^{\parallel}$. There is actually no issue because we are dealing with functions which are periodic both in $\boldsymbol{x}$ and t, generically denoted f, so that whatever the definition of the average $\langle \dots \rangle$ is we will have[1]

$$\langle \partial_t f \rangle = 0 \qquad \text{and} \qquad \Big\langle \boldsymbol{\nabla}^{\parallel} f \Big\rangle = 0. \tag{4.14}$$

However, we are considering a progressive wave so η actually depends only on the phase $\varphi = \boldsymbol{k} \cdot \boldsymbol{x} - \omega_1 t$. There exists non-linear progressive waves which are not periodic, like solitons and cnoidal waves, but we will not be concerned with them here. Thus, we conveniently take an average over the phase:

$$\langle f \rangle = \frac{1}{2\pi} \int_{-\pi}^{\pi} f d\varphi. \tag{4.15}$$

It has the advantage of formally obeying Reynolds averaging rules, especially (4.7).

The condition of small steepness apply to each harmonics: $\forall n \in \mathbb{N}^*,\ n|\boldsymbol{k} a_n| \ll 1$ and $n|\boldsymbol{k} b_n| \ll 1$. Along this line, let us mention an interesting result about the Fourier coefficients.

[1] It would not be the case if we had taken the bottom topography into account.

Lemma 2. *(Riemann-Lebesgue)*
If $\eta(\boldsymbol{x}, t=0)$ is bounded and integrable over $L_x \times L_y$, then $\lim_{n\to+\infty} a_n = 0$ and $\lim_{n\to+\infty} b_n = 0$.

Stricto sensu, it does not ensure the small steepness of higher harmonics. Nonetheless, it gives hopes about the existence of a class of functions whose Fourier sequence is absolutely decreasing faster than n. For instance, it is the case for the 2π-periodic function defined to be equal to x^2 on the interval $]-\pi, \pi]$. For such functions, it would be enough to impose $|\boldsymbol{k}a_1| \ll 1$ and $|\boldsymbol{k}b_1| \ll 1$ to make sure that all harmonics have a small steepness.

The condition of small steepness allows us to linearize the boundary conditions (4.1) and (4.3). Hence, we can restrict our attention to a plane wave $\eta(\boldsymbol{x}, t) = a\ \cos(\boldsymbol{k}\cdot\boldsymbol{x} - \omega t)$ and apply the superposition principle in the end. This wave propagates in the direction of $\boldsymbol{k}$ and is invariant by translation in the orthogonal direction. Thus, by setting up the direction of propagation along the x-axis one can simply consider a perturbation of the form $\eta(\boldsymbol{x}, t) = a\ \cos(kx - \omega t)$ invariant by translation in the y direction, which is in effect one-dimensional.

In that case, the velocity potential and subsequently the velocity field are known explicitly at the first order in ka. The phase velocity is denoted $\boldsymbol{c} = \frac{\omega}{k^2}\,\boldsymbol{k}$. One can show that the group velocity $\boldsymbol{c}_g = \boldsymbol{\nabla}_{\boldsymbol{k}}\,\omega$ is nicely related to $\boldsymbol{c}$ as

$$\boldsymbol{c}_g = \frac{1}{2}\left(\frac{2kh}{\sinh(2kh)} + \frac{1+3\left(\frac{k}{k_c}\right)^2}{1+\left(\frac{k}{k_c}\right)^2}\right)\boldsymbol{c}. \tag{4.16}$$

4.2.2 Wave energy

We treat separately the kinetic part and the contributions from gravity and surface tension.

1. The wave kinetic energy is

$$T = \left\langle \int_{-h}^{\eta} \frac{1}{2}\rho_w |\boldsymbol{u}|^2\, dz \right\rangle \simeq \int_{-h}^{0} \frac{1}{2}\rho_w \left\langle |\boldsymbol{u}|^2 \right\rangle dz = \frac{1}{4}\rho_w g a^2 \left(1 + \frac{\sigma k^2}{\rho_w g}\right). \tag{4.17}$$

   The integration from troughs to crests has been discarded because it would yield terms of third order in ka. The final expression was obtained thanks to the first order velocity field. Still, the following form (proved in section 4.2.9) will be useful:

$$T = \frac{1}{2}\rho_w \left\langle \phi|_{z=\eta} \partial_t \eta \right\rangle \simeq \frac{1}{2}\rho_w \left\langle \phi|_{z=0} \partial_t \eta \right\rangle. \tag{4.18}$$

   The approximation is for waves of small steepness; it gives back the final result of (4.17) when using the first order velocity potential.

2. The contribution of gravity to the wave potential energy is the difference between the gravitational energy of the water surface with and without waves:

$$V_g = \left\langle \int_{-h}^{\eta} \rho_w g z\, dz \right\rangle - \left\langle \int_{-h}^{0} \rho_w g z\, dz \right\rangle = \frac{1}{2}\rho_w g \left\langle \eta^2 \right\rangle = \frac{1}{4}\rho_w g a^2. \tag{4.19}$$

   Note that this result holds for waves of arbitrary steepness.

3. Surface tension is by definition an energy per unit area. Thus, to get its contribution to the wave potential energy one has to multiply it by the mean relative change of area. In the absence of waves, the water surface is flat and its area is simply $\Delta x \Delta y$. The wavy surface is represented by the Cartesian equation $z = \eta(\boldsymbol{x}, t)$. Hence,

$$V_\sigma = \sigma \left\langle \frac{\iint_{\mathcal{D}} \sqrt{1 + |\boldsymbol{\nabla}^{\parallel}\eta|^2}\, dxdy - \Delta x \Delta y}{\Delta x \Delta y} \right\rangle \simeq \sigma \left\langle \frac{\iint_{\mathcal{D}} \left(1 + \frac{1}{2}|\boldsymbol{\nabla}^{\parallel}\eta|^2\right) dxdy - \Delta x \Delta y}{\Delta x \Delta y} \right\rangle \tag{4.20}$$

$$= \frac{\sigma}{2}\,\frac{1}{\Delta x \Delta y} \iint_{\mathcal{D}} \left\langle |\boldsymbol{\nabla}^{\parallel}\eta|^2 \right\rangle dxdy = \frac{1}{4}\sigma (ka)^2. \tag{4.21}$$

   The Taylor expansion in equation (4.20) holds for waves of small steepness.

From equations (4.17), (4.19) and (4.21), we see that $T = V$ and so

$$E = \frac{1}{2}\rho_w g a^2 \left(1 + \frac{\sigma k^2}{\rho_w g}\right). \tag{4.22}$$

The equipartition of energy into its kinetic and potential components is true for any system undergoing small oscillations, as a consequence of the virial theorem for a harmonic potential.

Formula (4.22) can be written in a simple closed form inspired from (4.19) and (4.21):

$$E = \rho_w g \left\langle \eta^2 \right\rangle + \sigma \left\langle \left| \boldsymbol{\nabla}^{\parallel} \eta \right|^2 \right\rangle. \tag{4.23}$$

The reason why we skipped the horizontal integration in the second term is the following. Since we are considering perfectly periodic solutions of the water wave problem, we can restrict the horizontal domain to $L_x \times L_y$. Thus we recognize a spatial averaging of $\left\langle |\boldsymbol{\nabla}^{\parallel} \eta|^2 \right\rangle$. But as discussed in section 4.2.1, the spatial average is equivalent to $\langle \dots \rangle$. The conclusion then follows from the complementary Reynolds averaging rule (4.9).

Note that this closed form is consistent with Parseval theorem:

$$\left\langle \eta^2 \right\rangle = \frac{1}{2} \sum_{n=1}^{+\infty} \left(a_n^2 + b_n^2\right) \qquad \text{and} \qquad \left\langle \left| \boldsymbol{\nabla}^{\parallel} \eta \right|^2 \right\rangle = \frac{1}{2} \sum_{n=1}^{+\infty} \left\{ |\boldsymbol{k} a_n|^2 + |\boldsymbol{k} b_n|^2 \right\}. \tag{4.24}$$

4.2.3 Wave momentum

By definition, the wave momentum is

$$\boldsymbol{M} = \left\langle \int_{-h}^{\eta} \rho_w \boldsymbol{u} \, dz \right\rangle = \left\langle \int_{0}^{\eta} \rho_w \boldsymbol{u} \, dz \right\rangle + \int_{-h}^{0} \rho_w \langle \boldsymbol{u} \rangle \, dz. \tag{4.25}$$

The average commutes with the integration only in the second term because η is function of time, unlike h. Due to the irrotationality, one has $\langle \boldsymbol{u} \rangle = \langle \boldsymbol{\nabla} \phi \rangle = \boldsymbol{0}$ for progressive periodic waves of arbitrary steepness. Therefore, the region below wave troughs does not contribute to the wave momentum. Then,

$$\boldsymbol{M} = \left\langle \int_{0}^{\eta} \rho_w \boldsymbol{u} \, dz \right\rangle \simeq \left\langle \int_{0}^{\eta} \rho_w \boldsymbol{u}|_{z=0} \, dz \right\rangle = \rho_w \left\langle \eta \, \boldsymbol{\nabla} \phi \big|_{z=0} \right\rangle = \rho_w \left\langle \boldsymbol{\nabla}(\eta\phi) \big|_{z=0} - \phi|_{z=0} \, \boldsymbol{\nabla} \eta \right\rangle. \tag{4.26}$$

The approximation is for waves of small steepness. Besides, $\left\langle \boldsymbol{\nabla}(\eta\phi) \big|_{z=0} \right\rangle = \boldsymbol{0}$ for progressive periodic waves so that

$$\boldsymbol{M} = -\rho_w \left\langle \phi|_{z=0} \, \boldsymbol{\nabla}^{\parallel} \eta \right\rangle = \frac{1}{2} \rho_w \omega a^2 \operatorname{cotanh}(kh) \, \boldsymbol{e}_x. \tag{4.27}$$

We have replaced the gradient by its horizontal projection as $\partial_z \eta = 0$. This way, it makes clear that the wave momentum has no vertical component. The final expression was obtained thanks to the first order velocity potential.

A comparison between the explicit expressions (4.22) and (4.27) leads to the oustanding conclusion that

$$E = \boldsymbol{M} \cdot \boldsymbol{c}. \tag{4.28}$$

It is worth to remark that the explicit calculation of E and $\boldsymbol{M}$ is not necessary to infer this relation. Indeed, for a plane wave

$$\partial_t \eta + \boldsymbol{c} \cdot \boldsymbol{\nabla}^{\parallel} \eta = 0. \tag{4.29}$$

So one can get it directly from (4.18) and the first equality of (4.27).

4.2.4 Wave energy flux

The wave energy flux $\boldsymbol{\Phi}$ flux is in the direction of $\boldsymbol{k}$. So, let us compute the energy flux $\Delta y||\boldsymbol{\Phi}|| \equiv \Phi_S$ through a cross-sectional area S orthogonal to the direction of propagation. It is nothing but the mean rate of work on S of the excess pressure p_e due the presence of waves:

$$\Phi_S = \left\langle \iint_S p_e \boldsymbol{u} \cdot \boldsymbol{dS} \right\rangle = \Delta y \left\langle \int_{-h}^{\eta} p_e \partial_x \phi \, dz \right\rangle. \tag{4.30}$$

As for the kinetic energy, the integration from troughs to crests is discarded.

Bernoulli theorem together with Young-Laplace law yields[2]:

$$\partial_t \phi + \frac{1}{2} |\boldsymbol{\nabla} \phi|^2 + gz + \frac{p}{\rho_w} = -\frac{\sigma}{\rho_w} \boldsymbol{\nabla}^{\parallel} \cdot \left(\frac{\boldsymbol{\nabla}^{\parallel} \eta}{\sqrt{1 + |\boldsymbol{\nabla}^{\parallel} \eta|^2}} \right). \tag{4.31}$$

After linearization we get $p_e = -\rho_w \, \partial_t \phi - \sigma \, \nabla^{\parallel 2} \eta \equiv \rho_w \, c \, \partial_x \phi - \sigma \, \partial_x^2 \eta$. Then, a direct calculation with the first order horizontal velocity leads to

$$\boldsymbol{\Phi} = \frac{E}{2} \left(\frac{2kh}{\sinh(2kh)} + \frac{1 + 3\left(\frac{k}{k_c}\right)^2}{1 + \left(\frac{k}{k_c}\right)^2} \right) \boldsymbol{c}. \tag{4.32}$$

With the help of (4.16), we straightforwardly identify

$$\boldsymbol{\Phi} = E \, \boldsymbol{c}_g, \tag{4.33}$$

and conclude that wave energy is transported at the group velocity. This is not a surprise. We have indeed shown on general grounds in section 2.1.3 that the envelope of a wave packet, whose energy is proportional to the square of its amplitude, propagates at the group velocity.

This calculation yields further information on the partition and transport of energy.

1. For pure gravity waves, we readily see that the wave energy flux is reduced to

$$\boldsymbol{\Phi}_g = \int_{-h}^{0} \rho_w \left\langle |\boldsymbol{u}^{\parallel}|^2 \right\rangle dz \, \boldsymbol{c}. \tag{4.34}$$

   The integral is nothing but twice the horizontal wave kinetic energy, denoted $T^{\parallel}$. Since $E = 2T$, we get after comparison with (4.33)

$$\frac{c_g}{c} = \frac{T^{\parallel}}{T} \leqslant 1 \qquad \text{for gravity waves.} \tag{4.35}$$

   For deep water gravity waves, $\boldsymbol{c}_g = \frac{\boldsymbol{c}}{2}$ meaning that horizontal and vertical wave kinetic energies are equal. This equipartition is due to the absence of vertical length scale and not to the nature of the restoring force[3]. So we can generally state that

$$T^{\parallel} = \frac{T}{2} \qquad \Leftrightarrow \qquad \left\langle |\boldsymbol{u}^{\parallel}|^2 \right\rangle = \left\langle w^2 \right\rangle \qquad \text{in deep water.} \tag{4.36}$$

2. With the effect of surface tension, there is a supplementary term on the right-hand side of (4.35). In the deep water approximation, we can use (4.36) and find

$$\frac{c_g}{c} = \frac{1}{2} - \frac{\sigma}{2cT} \int_{-h}^{0} \left\langle \partial_x \phi \, \partial_x^2 \eta \right\rangle dz. \tag{4.37}$$

[2] According to Bernoulli theorem, there is also a function of time on the left-hand side of equation (4.31). Because of the gauge freedom on the velocity potential, this function could be set to zero as was done in the boundary condition (4.3).

[3] It is confirmed by a direct calculation with the first order velocity field.

For deep water capillary waves, $\boldsymbol{c}_g = \frac{3}{2}\boldsymbol{c}$ but in that case $T = V_\sigma$. We subsequently infer

$$-\sigma \int_{-h}^{0} \left\langle \partial_x \phi \, \partial_x^2 \eta \right\rangle dz = 2\, c\, V_\sigma. \tag{4.38}$$

So the mean rate of work of the capillary forces is unexpectedly equal to twice the product of the capillary wave energy by the the phase velocity. It is proved in section 4.2.9 that this result is an intrinsic property of the surface. Consequently, we can use it to express the ratio of group and phase velocities in terms of energetics:

$$\frac{c_g}{c} = \frac{T^{\parallel} + V_\sigma}{T} = 2\, \frac{T^{\parallel} + V_\sigma}{E}. \tag{4.39}$$

3. The above ratio can be readily expressed as

$$\frac{c_g}{c} = \frac{\Phi_S \mathcal{T}}{E L_x \Delta_y}, \tag{4.40}$$

which is the ratio of the energy crossing S during one period by the energy surplus in the volume $L_x \Delta_y S$ due the presence of waves. After (4.35), for gravity waves only a fraction of the energy content of a wave train of length L_x passes through S during its period $\mathcal{T}$. However, the inequality is reversed for pure for capillary waves. Indeed, equation (4.39) with $T = V_\sigma$ yields

$$\frac{c_g}{c} = 1 + \frac{T^{\parallel}}{T} \geqslant 1 \qquad \text{for capillary waves.} \tag{4.41}$$

It means that more energy passes through S than contained in the volume $L_x \Delta_y S$ ahead of it; a phenomenon called anomalous dispersion.

4. From the explicit expression (4.16), we readily get

$$\frac{c_g}{c} = \frac{kh}{\sinh(2kh)} + \frac{1}{2} \qquad \text{for gravity waves.} \tag{4.42}$$

After comparison with (4.35), we infer

$$\frac{kh}{\sinh(2kh)} = \frac{T^{\parallel}}{T} - \frac{1}{2}, \tag{4.43}$$

which is consistent with our conclusion (4.36) about the deep-water approximation. The form of (4.43) is independent of the restoring force so that we expect it to hold as well when including surface tension. This can be checked as follows. From (4.16), it comes

$$\frac{c_g}{c} = \frac{kh}{\sinh(2kh)} + \frac{3}{2} \qquad \text{for capillary waves,} \tag{4.44}$$

which after comparison with (4.41) indeed gives back (4.43).

4.2.5 Mean pressure and mean water level

The mean pressure $\langle p \rangle$ is obtained from the average vertical momentum equation:

$$\rho_w \left\langle \partial_t w \right\rangle + \left\langle \boldsymbol{\nabla}^{\parallel} \cdot \left(\rho_w w \boldsymbol{u}^{\parallel} \right) \right\rangle + \partial_z \left\langle p + \rho_w w^2 \right\rangle + \rho_w g = 0. \tag{4.45}$$

After the properties (4.14) of progressive periodic waves only remain the two last terms in that equation. Then, an integration from the bottom up to an arbitrary level below the mean water level $\langle \eta \rangle$ leads to

$$\langle p \rangle - p_0 + \rho_w \left\langle w^2 \right\rangle = 0 \qquad \text{on} \qquad [-h, \langle \eta \rangle], \tag{4.46}$$

where $p_0(z) = \rho_w g(\langle \eta \rangle - z)$ is the hydrostatic pressure, the atmospheric pressure being set to zero. Hence at any level below the water surface, the mean vertical flux of vertical momentum balances the weight of water above that level.

Besides, the average dynamical boundary condition (4.3) is

$$\langle \partial_t \phi \rangle + \frac{1}{2} \left\langle |\boldsymbol{\nabla}\, \phi|^2 \right\rangle + g \langle \eta \rangle + \frac{\langle p \rangle}{\rho_w} = -\frac{\sigma}{\rho_w} \left\langle \boldsymbol{\nabla}^{\parallel} \cdot \left(\frac{\boldsymbol{\nabla}^{\parallel} \eta}{\sqrt{1 + |\boldsymbol{\nabla}^{\parallel} \eta|^2}} \right) \right\rangle \qquad \text{at} \qquad z = \langle \eta \rangle . \tag{4.47}$$

Invoking (4.14) once more, we get the following relation between mean pressure and mean water level:

$$\frac{1}{2} \left\langle |\boldsymbol{u}^{\parallel}|^2 + w^2 \right\rangle + g \langle \eta \rangle + \frac{\langle p \rangle}{\rho_w} = 0 \qquad \text{at} \qquad z = \langle \eta \rangle . \tag{4.48}$$

So as to check its consistency with the natural balance expressed by (4.46), let us evaluate the latter at the mean water level. It gives

$$\langle p \rangle + \rho_w \left\langle w^2 \right\rangle = 0 \qquad \text{at} \qquad z = \langle \eta \rangle . \tag{4.49}$$

The only way to reconciliate (4.48) and (4.49) is to consider deep water waves. Then, after the key relation (4.36), the quadratic terms in (4.48) equally contribute. Consequently, one has to take $\langle \eta \rangle = 0$ in deep water. Since waves usually travel from the middle of the ocean to the coast, this condition extends to finite depth. It implies

$$p_0(z) = -\rho_w g z \qquad \forall z \in [-h, 0]. \tag{4.50}$$

4.2.6 Radiation stress tensor

For the sake of simplicity, the effect of surface tension is discarded in this section.

The wave momentum flux $\mathbb{S}$ is called 'radiation stress tensor'. We recall that the inviscid momentum flux in an incompressible fluid is $\rho \boldsymbol{u} \otimes \boldsymbol{u} + (p - p_0)\mathbb{1}$, with p_0 given by (4.50). Thus, the excess momentum flux due to the presence of waves is purely horizontal and expressed in the canonical basis $(\boldsymbol{e}_x, \boldsymbol{e}_y)$ as

$$S_{ij} = \left\langle \int_{-h}^{\eta} (\rho_w u_i u_j + p \delta_{ij})\, dz \right\rangle - \int_{-h}^{0} p_0 \delta_{ij}\, dz, \qquad i, j = 1, 2. \tag{4.51}$$

We have substracted the hydrostatic term which was already contributing before the surface got disturbed. As previously, the integration of the quadratic term from troughs to crests can be discarded. Hence,

$$S_{ij} \simeq \int_{-h}^{0} \rho_w \langle u_i u_j \rangle dz + \int_{-h}^{0} (\langle p \rangle - p_0) \delta_{ij}\, dz + \left\langle \int_{0}^{\eta} p\, dz \right\rangle \delta_{ij}. \tag{4.52}$$

The first integral is evaluated using the first order velocity field. Since the direction of propagation has been set up along the x-axis, it is just

$$\int_{-h}^{0} \rho_w \left\langle (\partial_x \phi)^2 \right\rangle dz\ \delta_{i1}\delta_{j1} \equiv 2T^{\parallel} \delta_{i1}\delta_{j1}. \tag{4.53}$$

With the help of formula (4.49), we find

$$\int_{-h}^{0} (\langle p \rangle - p_0) dz = -\rho_w \int_{-h}^{0} \left\langle w^2 \right\rangle dz \equiv 2(T^{\parallel} - T) = 2T^{\parallel} - E. \tag{4.54}$$

To evaluate the last term in (4.52), we approximate the dynamical pressure near the disturbed surface by its hydrostatic counterpart. Setting the atmospheric pressure to zero, it leads to

$$p(\boldsymbol{r}, t) \simeq \rho_w g \big(\eta(\boldsymbol{x}, t) - z\big) \qquad \Rightarrow \qquad \left\langle \int_{0}^{\eta} p\, dz \right\rangle = \frac{E}{2}. \tag{4.55}$$

In the end, using the energetic interpretation (4.35) of the ratio of group and phase velocities, the radiation stress tensor in the canonical basis is found to be

$$\mathbb{S} = \begin{pmatrix} E\big(\frac{2c_g}{c} - \frac{1}{2}\big) & 0 \\ 0 & E\big(\frac{c_g}{c} - \frac{1}{2}\big) \end{pmatrix}. \tag{4.56}$$

Otherwise, an intrinsic expression is

$$S_{ij} = \frac{E c_g}{c} \frac{k_i k_j}{|\boldsymbol{k}|^2} + E\left(\frac{c_g}{c} - \frac{1}{2}\right) \delta_{ij}. \tag{4.57}$$

For deep water gravity waves,

$$\mathbb{S} = \frac{E}{2}\, \frac{\boldsymbol{k} \otimes \boldsymbol{k}}{|\boldsymbol{k}|^2}. \tag{4.58}$$

4.2.7 A heuristic note on tsunamis

Let us consider consider a long wave generated by an earthquake at a point A in the middle of the ocean and propagating along the x-axis until a point B on the coast. Let Π_A and Π_B be parallel vertical planes containing A and B respectively, and having the same lateral extension Δy. Assuming neither further wave generation nor dissipation, the energy that enters through Π_A in the volume of water delimited by those planes must be equal to the energy that goes out through Π_B. In other words, the energy flux is conserved:

$$\Phi_{\Pi_A} = \Phi_{\Pi_B} \qquad \Rightarrow \qquad (c_g E)_A = (c_g E)_B. \tag{4.59}$$

The point A is located in deep water, thus $c_{gA} = \frac{1}{2}\sqrt{\frac{g}{k}}$ is large because the wave is long (k small). On the contrary, the point B is located in very shallow water (h tiny) so that $c_{gB} = \sqrt{gh}$ is very small. In both cases, the energy is proportional to the square of the wave amplitude. Since the group velocity is considerably decreasing from A to B, the conservation law (4.59) implies a huge increase of the wave amplitude. This phenomenon is called wave shoaling. It provides a qualitative explanation for tsunamis' formation. A more quantitative one requires to take non-linear effects into account. From the point of view of wave-wave interaction, they are expected to be very strong in shallow water; as there is no dispersion, waves will interact on a short time scale. Note that the wave amplitude would grow even more from A to B if the lateral extension of Π_B was smaller than the lateral extension of Π_A. Thus, the effect of wave shoaling is amplified in narrow shores.

4.2.8 Key points

i) The kinetic energy and the potential energy equally contribute to the wave energy.

ii) The ratio of the wave energy and the wave momentum is equal to the phase velocity.

iii) The energy propagates at the group velocity.

4.2.9 Proofs

Proof of equation (4.18)

Equation (4.18) is proved for an unven bottom and a statistically homogeneous random wave field.

Proof. (Adapted from [37])
For convenience, let us define $I = \int_{-h}^{\eta} |\,\boldsymbol{\nabla}\,\phi|^2 dz$. The identity $\boldsymbol{\nabla}\cdot(\phi\,\boldsymbol{\nabla}\,\phi) = |\,\boldsymbol{\nabla}\,\phi|^2 + \phi\nabla^2\phi$ together with the Laplace equation leads to

$$I = \int_{-h}^{\eta} \boldsymbol{\nabla}\cdot(\phi\,\boldsymbol{\nabla}\,\phi)\,dz = \int_{-h}^{\eta} \boldsymbol{\nabla}^{\parallel}\cdot(\phi\,\boldsymbol{\nabla}^{\parallel}\,\phi)\,dz + \Big[\phi\partial_z\phi\Big]_{-h}^{\eta}. \tag{4.60}$$

Since

$$\boldsymbol{\nabla}^{\parallel}\cdot\int_{-h}^{\eta}\phi\,\boldsymbol{\nabla}^{\parallel}\,\phi\,dz = \int_{-h}^{\eta}\boldsymbol{\nabla}^{\parallel}\cdot(\phi\,\boldsymbol{\nabla}^{\parallel}\,\phi)\,dz + \boldsymbol{\nabla}^{\parallel}\,\eta\cdot\Big(\phi\,\boldsymbol{\nabla}^{\parallel}\,\phi\Big)\Big|_{z=\eta} + \boldsymbol{\nabla}^{\parallel}\,h\cdot\Big(\phi\,\boldsymbol{\nabla}^{\parallel}\,\phi\Big)\Big|_{z=-h}, \tag{4.61}$$

$$I = \Big\{\phi\Big(\partial_z\phi - \boldsymbol{\nabla}^{\parallel}\,\phi\cdot\boldsymbol{\nabla}^{\parallel}\,\eta\Big)\Big\}\Big|_{z=\eta} + \Big\{\phi\Big(\partial_z\phi + \boldsymbol{\nabla}^{\parallel}\,\phi\cdot\boldsymbol{\nabla}^{\parallel}\,h\Big)\Big\}\Big|_{z=-h} + \boldsymbol{\nabla}^{\parallel}\cdot\int_{-h}^{\eta}\phi\,\boldsymbol{\nabla}^{\parallel}\,\phi\,dz. \tag{4.62}$$

After invoking the kinematic boundary conditions (4.1) and (4.2), we eventually obtain

$$T = \frac{1}{2}\rho_w\,\langle I\rangle = \frac{1}{2}\rho_w\,\langle\phi|_{z=\eta}\partial_t\eta\rangle + \frac{1}{2}\rho_w\,\boldsymbol{\nabla}^{\parallel}\cdot\left\langle\int_{-h}^{\eta}\phi\,\boldsymbol{\nabla}^{\parallel}\,\phi\,dz\right\rangle. \tag{4.63}$$

As discussed in section 4.2.1, the second term vanishes for progressive periodic waves. It actually also does for a statistically homogeneous random wave field because the average is then independent of $\boldsymbol{x}$. □

Proof of equation (4.38)

Equation (4.38) is proved for a statistically homogeneous random wave field.

Proof.

$$-\sigma \int_{-h}^{0} \big\langle \partial_x\phi \; \partial_x^2\eta \big\rangle \, dz = -\sigma \int_{-h}^{0} \big\langle \partial_x(\partial_x\phi \; \partial_x\eta) - \partial_x^2\phi \; \partial_x\eta \big\rangle \, dz \equiv -\sigma \left\langle \partial_x\eta \int_{-h}^{0} \partial_z^2\phi \; dz \right\rangle \tag{4.64}$$

Indeed $\langle \partial_x(\partial_x\phi \; \partial_x\eta) \rangle = 0$ with the same arguments as given in the end of section (4.2.9). Furthermore, we made use of the 2-dimensional Laplace equation to introduce a vertical derivative. After integration and enforcing the (linearized) kinematic boundary conditions (4.1) and (4.10), we obtain

$$-\sigma \int_{-h}^{0} \big\langle \partial_x\phi \; \partial_x^2\eta \big\rangle \, dz = -\sigma \, \langle \partial_x\eta \; \partial_t\eta \rangle = \sigma c \big\langle (\partial_x\eta)^2 \big\rangle \equiv 2 \; c \; V_\sigma. \tag{4.65}$$

□

4.3 Waves in a slowly varying medium

In this section based on the book by Bühler [38], we study the effect of bottom topography and currents. Since the vertical coordinate is not involved, we skip the symbol $\|$ from the horizontal projection of the gradient.

4.3.1 Ray theory

We studied in section 2.1.3 the propagation of a weakly non-linear wave packet in a dispersive medium. We required the wave packet to be spectrally narrow so that it could be represented by a plane wave whose amplitude is slowly varying in space and subsequently in time. Here, we take a different perspective and consider the linear evolution of a plane wave in a slowly varying medium. Hence, not only its amplitude is a function of space and time but also its wavenumber and angular frequency. It is represented by

$$\eta(\boldsymbol{x}, t) = \Re\Big\{ A(\boldsymbol{x}, t) \; e^{iS(\boldsymbol{x},t)} \Big\}, \tag{4.66}$$

where $S(\boldsymbol{x}, t)$ is a phase function. The key assumption of a slowly varying medium entails that the wave train looks like a plane wave at every $(\boldsymbol{x}, t)$ so that one can define a local wavenumber and a local angular frequency as follows:

$$dS = \boldsymbol{k} \cdot \boldsymbol{dx} - \omega dt \qquad \Leftrightarrow \qquad \boldsymbol{k}(\boldsymbol{x}, t) = \boldsymbol{\nabla} \, S \qquad \text{and} \qquad \omega(\boldsymbol{x}, t) = -S_t. \tag{4.67}$$

The scale separation could be made explicit by writing $S = \beta^{-1}\tilde{S}$ with $\beta \ll 1$. Then, one recognizes the leading order of a WKB approximation. As it was first developed in geometric optics, this standard procedure is called ray theory. Note that $|\boldsymbol{k}|$ and ω are of order ϵ^{-1} by construction, thus for consistency the dispersion relation should be such that high angular frequencies are proportional to high wavenumbers. This is the case for water waves.

It is useful to remark that $\boldsymbol{\nabla} \times \boldsymbol{k} = \boldsymbol{0}$, implying

$$\frac{\partial k_i}{\partial x_j} = \frac{\partial k_j}{\partial x_i}. \tag{4.68}$$

A wave front is defined by $S(\boldsymbol{x}, t) = cst$ or equivalently $dS = 0$, thus it propagates at speed $\frac{\boldsymbol{dx}}{dt} = \frac{\omega}{|\boldsymbol{k}|^2}\boldsymbol{k}$ which is the local phase velocity. We get back to its original definition as speed of a wave crest. Indeed, the equation

$$\big(\partial_t \, \boldsymbol{\nabla} - \boldsymbol{\nabla} \, \partial_t\big) S(\boldsymbol{x}, t) = \boldsymbol{0} \qquad \Leftrightarrow \qquad \partial_t \boldsymbol{k} + \boldsymbol{\nabla} \, \omega = \boldsymbol{0} \tag{4.69}$$

is often called 'conservation law for wave crests'.

Because of dispersion, there exists a function $\Omega(\boldsymbol{k}, \boldsymbol{x}, t)$ such that

$$\omega(\boldsymbol{x}, t) = \Omega\big(\boldsymbol{k}(\boldsymbol{x}, t), \boldsymbol{x}, t\big). \tag{4.70}$$

We now have to write dynamical equations for $\boldsymbol{k}$ and ω. To do so, let us explicit the gradient in equation (4.69) with the help of (4.68):

$$\frac{\partial \omega}{\partial x_i} = \frac{\partial \Omega}{\partial x_i} + \frac{\partial \omega}{\partial k_j}\frac{\partial k_j}{\partial x_i} \equiv \frac{\partial \Omega}{\partial x_i} + \frac{\partial \omega}{\partial k_j}\frac{\partial k_i}{\partial x_j} \qquad \Rightarrow \qquad \partial_t \boldsymbol{k} + \big(\boldsymbol{c}_g \cdot \boldsymbol{\nabla}\big)\boldsymbol{k} = -\partial_{\boldsymbol{x}}\Omega, \tag{4.71}$$

where $\boldsymbol{c}_g(\boldsymbol{x}, t) = \partial_{\boldsymbol{k}}\Omega$ is the local group velocity. The function Ω being known, we have got a quasi-linear PDE for $\boldsymbol{k}(\boldsymbol{x}, t)$, which can be conveniently solved thanks to the method of characteristics. They are special lines along which the PDE can be solved by integrating a system of ODEs. In our case, the characteristics curves are parametrized by τ in the space $(\boldsymbol{x}, t, \boldsymbol{k})$ and solutions of

$$\begin{cases} \frac{d\boldsymbol{x}}{d\tau} = \boldsymbol{c}_g \\ \frac{dt}{d\tau} = 1 \\ \frac{d\boldsymbol{k}}{d\tau} = -\partial_{\boldsymbol{x}}\Omega \end{cases} \qquad \Leftrightarrow \qquad \begin{cases} \frac{d\boldsymbol{x}}{dt} = \partial_{\boldsymbol{k}}\Omega \\ \frac{d\boldsymbol{k}}{dt} = -\partial_{\boldsymbol{x}}\Omega \end{cases} . \tag{4.72}$$

In this special case, t is used as a parameter and is no more an independent variable. So we have moved to the Lagrangian point of view. The connexion with the original Eulerian point of view is made by introducing a directional derivative along the characteristics: $\frac{d}{dt} = \partial_t + \boldsymbol{c}_g \cdot \boldsymbol{\nabla}$. In fact, it would be more correct to say that we have moved to the 'Hamiltonian' point of view. The function $\Omega(\boldsymbol{k}, \boldsymbol{x}, t)$ can indeed be regarded as a Hamiltonian function and $(\boldsymbol{x}, \boldsymbol{k})$ as points in a phase space; the right-hand side of (4.72) are the corresponding Hamilton's equations of motion. Moreover,

$$\partial_t S + \Omega\big(\boldsymbol{\nabla} S, \boldsymbol{x}, t\big) = 0 \tag{4.73}$$

can be identified as a Hamilton-Jacobi equation. Let us go further and make the substitution $S \to \hbar S$, with $\hbar$ the reduced Planck constant. First of all, $\hbar S$ appears to be the least action (Hamilton's principle). Secondly after the Planck-Einstein formula, $\hbar\Omega$ can be interpreted as the energy of a corpuscule while $\hbar\boldsymbol{k}$ stands for its momentum according to the de Broglie formula. Thus, we have a complete picture of the wave-particle duality. Coming back to the original approach of geometric optics, we define rays as the solution $\boldsymbol{x}(t)$ in the physical space. Finally, we calculate the time derivative of ω along a ray:

$$\frac{d\omega}{dt} = \partial_t\Omega + \partial_{\boldsymbol{k}}\Omega\,\frac{d\boldsymbol{x}}{dt} + \partial_{\boldsymbol{x}}\Omega\,\frac{d\boldsymbol{k}}{dt} \equiv \partial_t\Omega. \tag{4.74}$$

Hence, when the dispersion relation does not depend explicitly on time, the angular frequency is conserved along a ray and transported at the group velocity. Then one ray corresponds to one angular frequency, like one trajectory corresponds to one energy in conservative Hamiltonian mechanics. Similarly, when the dispersion relation does not depend explicitly on the position, the wavenumber is conserved along a ray and transported at the group velocity. These standard results could be directly inferred from the famous Noether's theorem.

The variation of $\boldsymbol{k}$ along a ray, which is subsequently not straight, is a refraction. For water waves, it comes from bottom variation and/or the presence of a non-uniform current.

4.3.2 Bottom refraction

In this section, we consider the effect of bottom variation through the function $h(\boldsymbol{x})$. Let Λ be a horizontal length scale, then the variation looks slow to the waves if $|\boldsymbol{k}|\Lambda \gg 1$. Besides, they effectively 'feel' that variation if at most $|\boldsymbol{k}|h_0 = \mathcal{O}(1)$ where h_0 is a characteristic depth. Thus, the appropriate small parameter for the WKB approximation is $\beta = \frac{h_0}{\Lambda} \ll 1$. It can be shown [39] that the local dispersion relation keeps the same form as when the depth is constant:

$$\omega^2(\boldsymbol{x}, t) = g|\boldsymbol{k}(\boldsymbol{x}, t)| \tanh\big(|\boldsymbol{k}(\boldsymbol{x}, t)|h(\boldsymbol{x})\big)\left(1 + \frac{\sigma|\boldsymbol{k}(\boldsymbol{x}, t)|^2}{\rho_w g}\right). \tag{4.75}$$

Since $\partial_t h = 0$, we have $\partial_t \Omega = 0$ and ω is conserved along a ray. In the standard case when $\partial_y h = 0$, we also have $\partial_y \Omega = 0$ which implies that the wavenumber l in the y-direction is conserved along a ray too. Let us introduce the angle $\alpha = (\boldsymbol{e}_x, \boldsymbol{k})$, then $l = |\boldsymbol{k}| \sin(\alpha)$. Combining the conservation of l and $\omega = |\boldsymbol{k}|c$, we eventually get

$$\frac{\sin(\alpha)}{c} = cst, \qquad \text{along a ray.} \tag{4.76}$$

This is nothing but the Snell-Descartes law for refraction. The Cartesian equation of rays can be obtained as follows:

$$\begin{cases} \frac{dx}{dt} = \partial_x \Omega = \frac{\partial \Omega}{\partial |\boldsymbol{k}|} \frac{\partial |\boldsymbol{k}|}{\partial x} = \frac{\partial \Omega}{\partial |\boldsymbol{k}|} \frac{k}{|\boldsymbol{k}|} \\ \frac{dy}{dt} = \partial_y \Omega = \frac{\partial \Omega}{\partial |\boldsymbol{k}|} \frac{\partial |\boldsymbol{k}|}{\partial y} = \frac{\partial \Omega}{\partial |\boldsymbol{k}|} \frac{l}{|\boldsymbol{k}|} \end{cases} \qquad \Rightarrow \qquad \frac{dy}{dx} = \frac{l}{k}. \tag{4.77}$$

l is a constant while $k(x, y)$ should be extracted (maybe numerically) from the depth-dependent dispersion relation for a given value of ω. One eventually gets a first order non-linear ODE whose resolution might be challenging.

4.3.3 Current refraction

In the presence of a uniform current $\boldsymbol{U}$, one should distinguish the intrinsic angular frequency $\hat{\omega}$, measured in a frame moving with the current, from the absolute frequency ω, measured by a steady observer. They are different by a Doppler shift: $\omega = \hat{\omega} + \boldsymbol{k} \cdot \boldsymbol{U}$. It is obviously $\hat{\omega}$ that obeys the dispersion relation. The corresponding absolute and intrinsic group velocities are $\boldsymbol{c}_g$ and $\hat{\boldsymbol{c}}_g$, such that $\boldsymbol{c}_g = \hat{\boldsymbol{c}}_g + \boldsymbol{U}$.

In this section, we want to study the effect of a slowly varying current $\boldsymbol{U}(\boldsymbol{x}, t)$. Vertical variations may result in the growth of waves, but this is beyond the scope of this work. We add a local Doppler shift to the ray theory through a redefinition of the function Ω:

$$\Omega(\boldsymbol{k}, \boldsymbol{x}, t) = \hat{\Omega}(\boldsymbol{k}, \boldsymbol{x}, t) + \boldsymbol{k} \cdot \boldsymbol{U}(\boldsymbol{x}, t). \tag{4.78}$$

As a direct consequence, the directional derivative along the characteristics becomes $\frac{d}{dt} = \partial_t + (\hat{\boldsymbol{c}}_g + \boldsymbol{U}) \cdot \boldsymbol{\nabla}$ with $\hat{\boldsymbol{c}}_g = \partial_{\boldsymbol{k}} \hat{\Omega}$. The corresponding Hamilton's equations are

$$\begin{cases} \frac{d\boldsymbol{x}}{dt} = \partial_{\boldsymbol{k}} \hat{\Omega} + \boldsymbol{U} \\ \frac{d\boldsymbol{k}}{dt} = -\partial_{\boldsymbol{x}} \Omega - (\boldsymbol{\nabla} \boldsymbol{U})^t \cdot \boldsymbol{k} \end{cases}. \tag{4.79}$$

The supplementary term in the second equation is responsible for current refraction.

Chapter 5

Summary and outlook

The scientific history of waves began about two centuries ago with the linear theory of water waves. Once classified in terms of their restoring force and water depth, non-linear effects started to be explored. For deep water gravity waves of small steepness, Stokes calculated a dispersion relation which depends on the wave amplitude. He also showed the existence of a wave-induced current, the Stokes drift. However, Stokes waves are not commonly observed and it is only in the late sixties that Benjamin and Feir showed that they are actually unstable. This phenomenon, called modulational instability, was realized to be a consequence of the coupling between dispersion and weak non-linearity, and can be universally described by a non-linear Schrödinger equation. It is also a paradigmatic example of a four-wave resonant interaction. Indeed, one can explain thanks to Zakharov equation the time evolution of the spectral amplitude in terms of wave-wave interactions. For deep water gravity waves, triadic resonant interactions are absent because the linear dispersion relation is a concave function. Concavity also appears to be a necessary condition for side-band instability. The framework of wave-wave interaction provides a general description of weakly non-linear waves. However, to study an ensemble of waves or a system with random initial conditions, a statistical description is needed. The solution is the wave turbulence theory, which basically gives the time evolution of the second moment. Nazarenko [40] defines it as 'the out-of-equilibrium statistical mechanics of random non-linear waves'.

It was shown by Phillips in 1957 that a turbulent wind generates a continuous spectrum of waves. Therefore, ocean waves seem to go into the class of systems addressed by wave turbulence. But there are other processes to take into account prior to wave-wave interaction. One of them is wind-wave interaction, which we believe to be the most important. So far, the two have been decoupled: a term yielding an exponential growth, based on the theory of Miles (1957), is simply added in the equation of wave turbulence. Miles' idea was to regard the waves as perturbations of the air flow and then use the theory of hydrodynamic stability to get the growth rate. The wind being turbulent, it is averaged over a time scale much smaller than the period of the waves so that a logarithmic profile can eventually be used and then treated as a parallel shear flow. The subsequent eigenvalue problem was too difficult to solve but there is a natural small parameter in the wind-waves system, the air-water density ratio, which allows a perturbative resolution. Note that this small parameter is at the origin of the weak coupling between the air and water layers which entails the small steepness of the waves. Miles' formula for the growth rate of wind waves requires the solution of a linear singular boundary value problem. Since the singularity is regular, we used the Frobenius' series to develop a simple numerical scheme for solving problems of that class. Then we computed Miles' growth rate and confronted it to the existing observational data. Despite of the scattering of the data, there is a good agreement between theory and experiments over almost two decades. Furthermore, a power law seems to emerge in this range. Nonetheless, Miles' theory predicts a maximum which is not observed. So as to understand these facts, in addition to what characteristics the wind profile should have to make the waves grow, an approximate analytical expression of the growth rate for a generic profile is desirable. Therefore, we initiated the resolution of the boundary value problem for short and long waves. So far, the calculations are complete for short waves: at leading order, the solution is equal to the free-stream solution e^{-kz}. Furthermore, we proved that this result, also supported by numerics, is independent of the wind profile and of the dispersion relation. The latter lets us think about a generalization of Miles' theory to capillary waves. For long waves, the situation is trickier. Indeed, we have separated the domain into two regions but are so far able to provide asymptotic solutions for a generic profile only in the region containing the singularity. Although the behaviour of the solution should be anyway exponential at infinity, in the overlapping region it strongly

depends on the profile. The divergence of the logarithmic profile at infinity is challenging, but progress could be made with the exponential profile which is bounded. A patching method then yielded reasonably good results when compared with the exact numerical solution. Hence, these asymptotic results are encouraging. They will provide a better insight on Miles' theory. Furthermore, they could be used to study the quasi-linear model of Janssen [41] describing the feedback of growing ocean waves on the wind profile. Indeed, the wave spectrum is continuous so that there is an interaction between the different critical levels, which is a counterpart of wave turbulence.

Chapter 6

Appendix: Figures supporting the asymptotic results of section 3.3

Here is a series of plots comparing the asymptotic solution of the boundary value problem (3.3) for short and long waves and the solution computed with the help of our numerical scheme. We vary both the Froude number Fr and the wavenumber k. In the case of short waves, we present solutions for the exponential profile U_1 as well as for logarithmic profile U_2, defined in section 3.1.

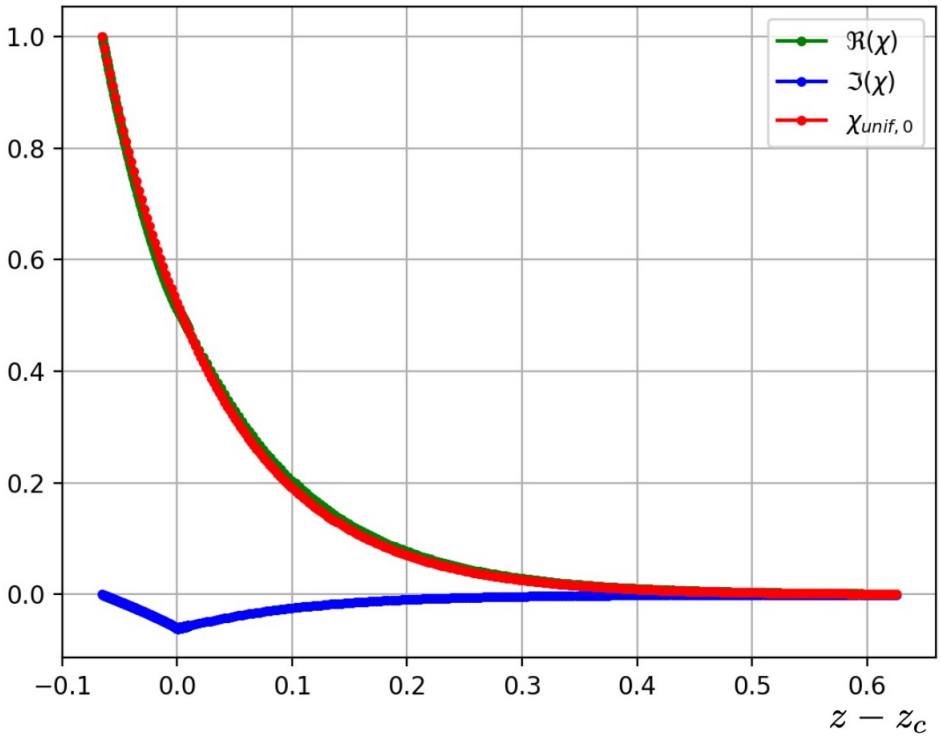

Figure 6.1: Solution for the exponential profile and $k = 10$, $Fr = 5$.

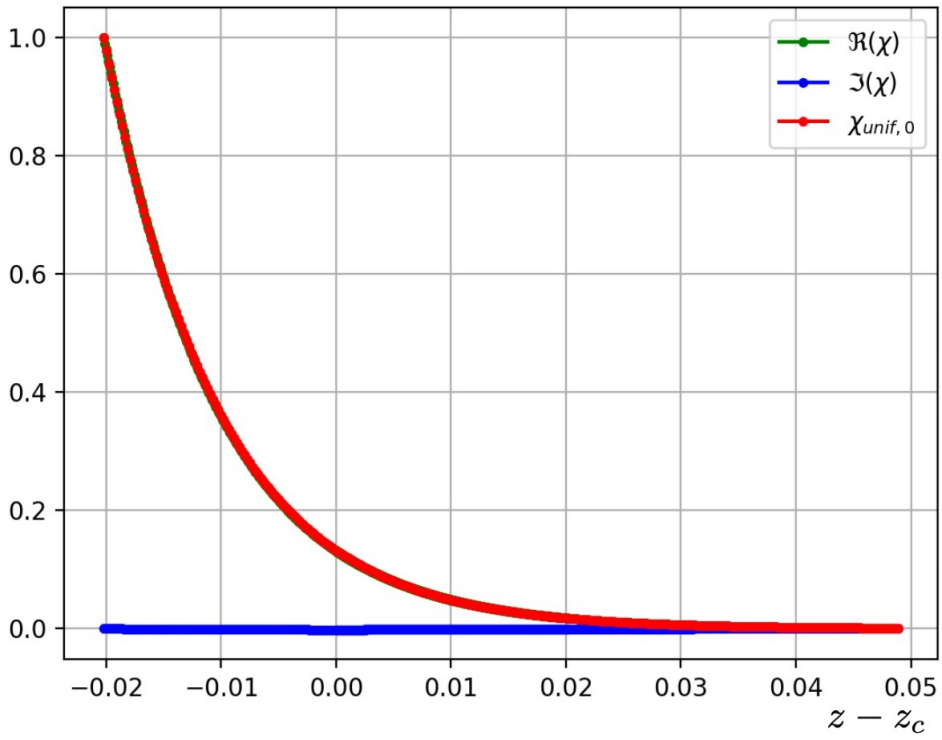

Figure 6.2: Solution for the exponential profile and $k = 100$, $Fr = 5$.

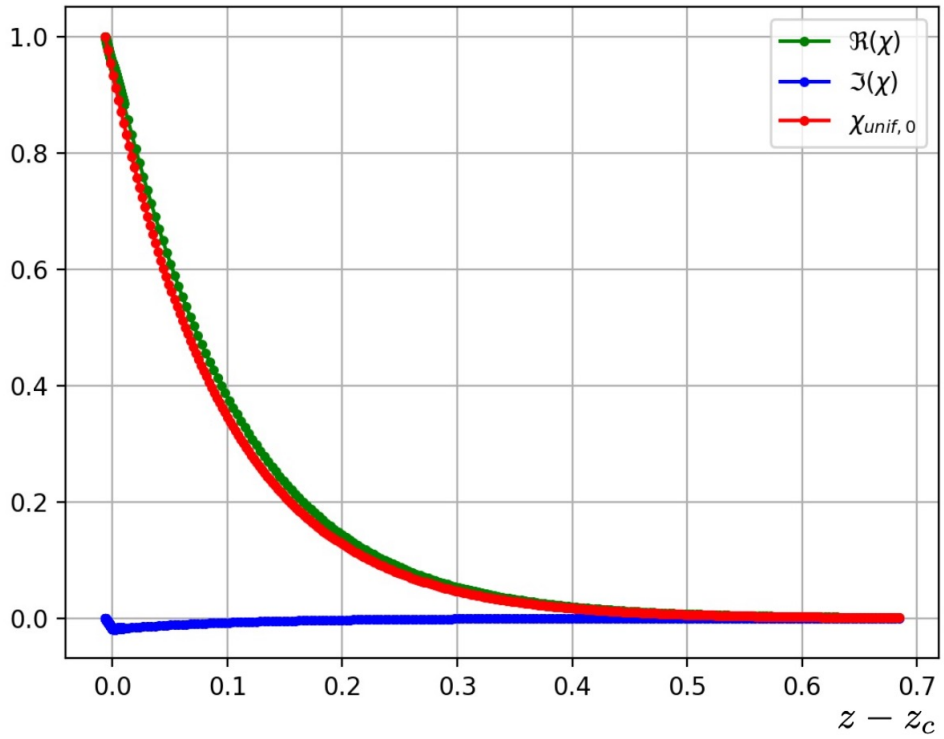

Figure 6.3: Solution for the exponential profile and $k = 10$, $Fr = 50$.

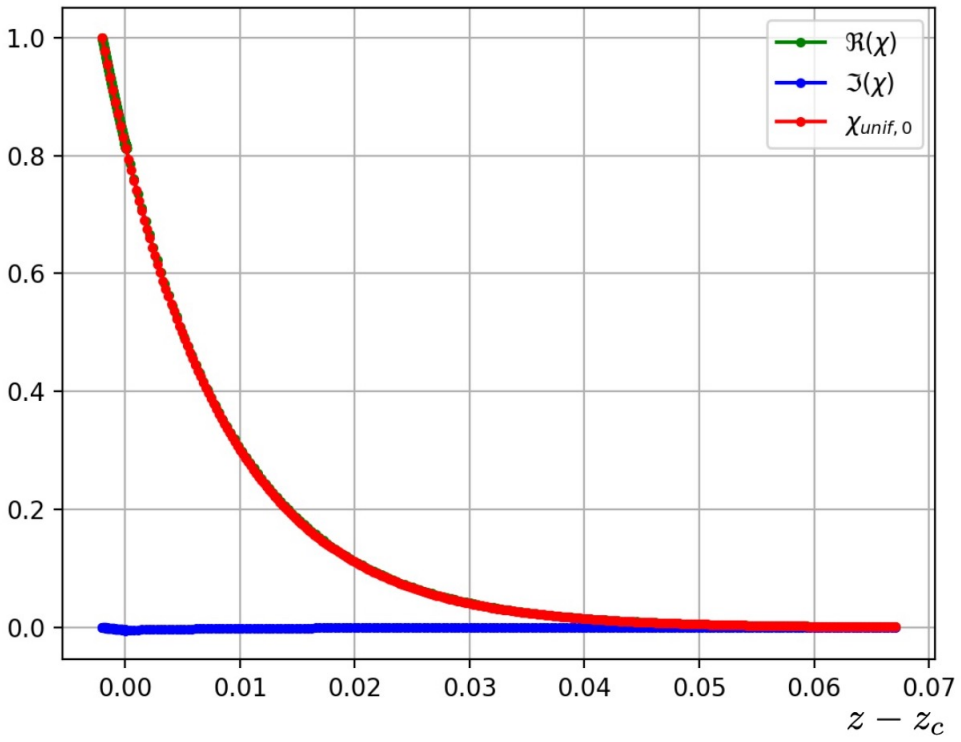

Figure 6.4: Solution for the exponential profile and $k = 100$, $Fr = 50$.

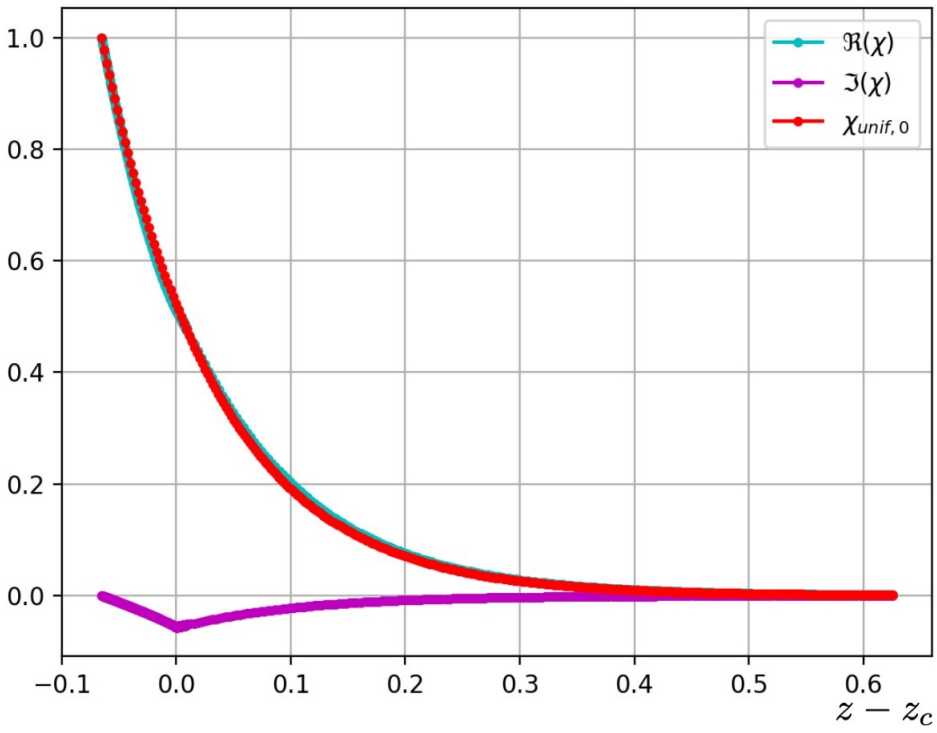

Figure 6.5: Solution for the logarithmic profile and $k = 10$ and $Fr = 5$.

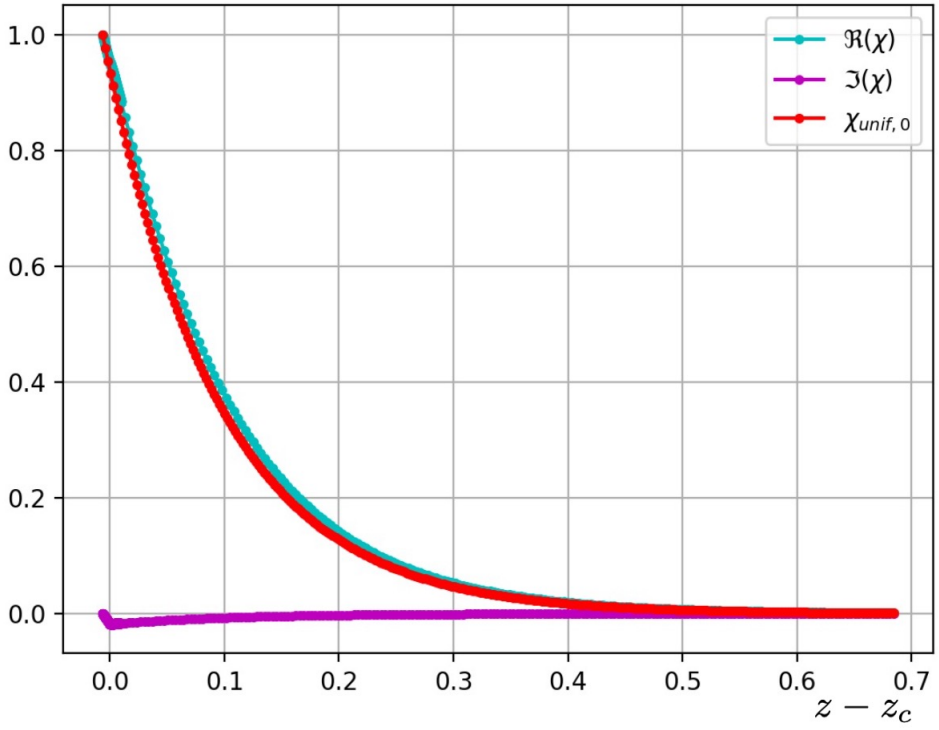

Figure 6.6: Solution for the logarithmic profile and $k = 10$ and $Fr = 50$.

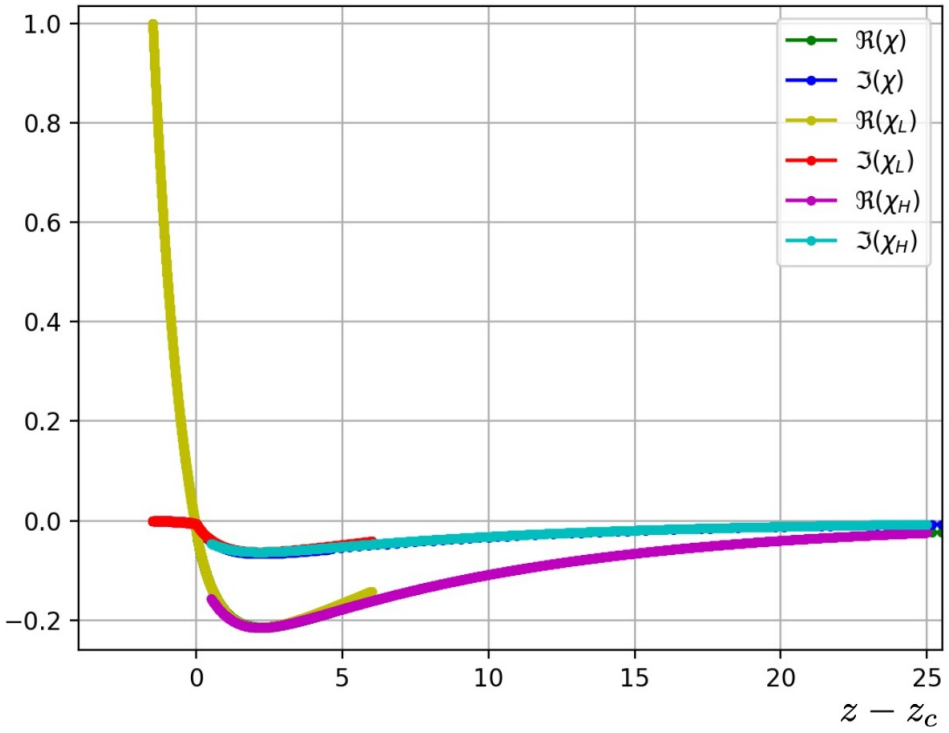

Figure 6.7: Solution for the exponential profile and $k = 0.1$ and $z_c = 1.5$.

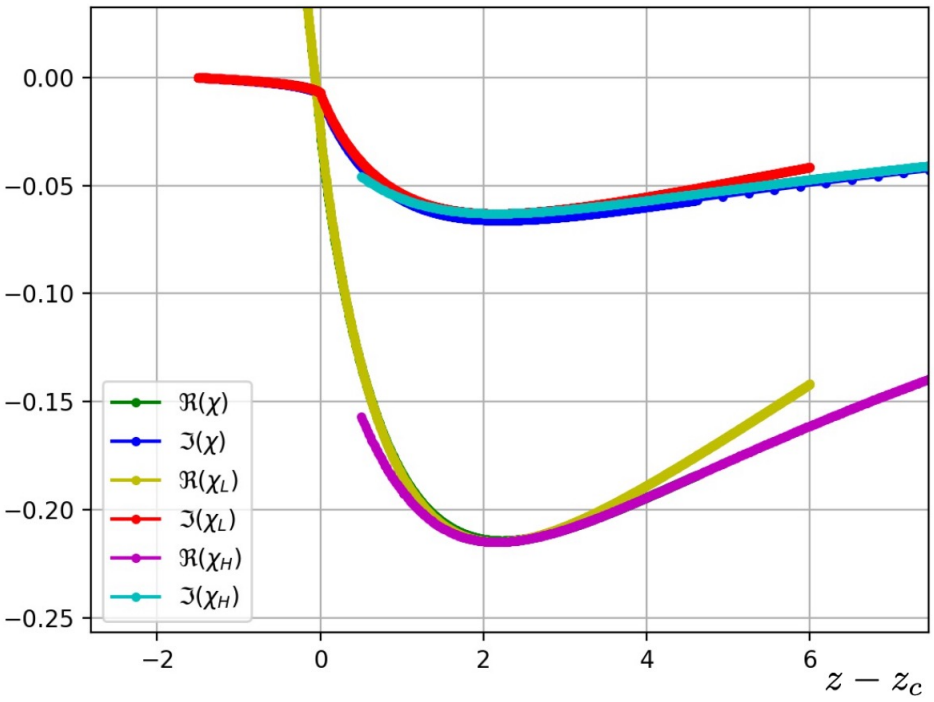

Figure 6.8: Zoom on the minimum (where the patching is made) in figure 6.7.

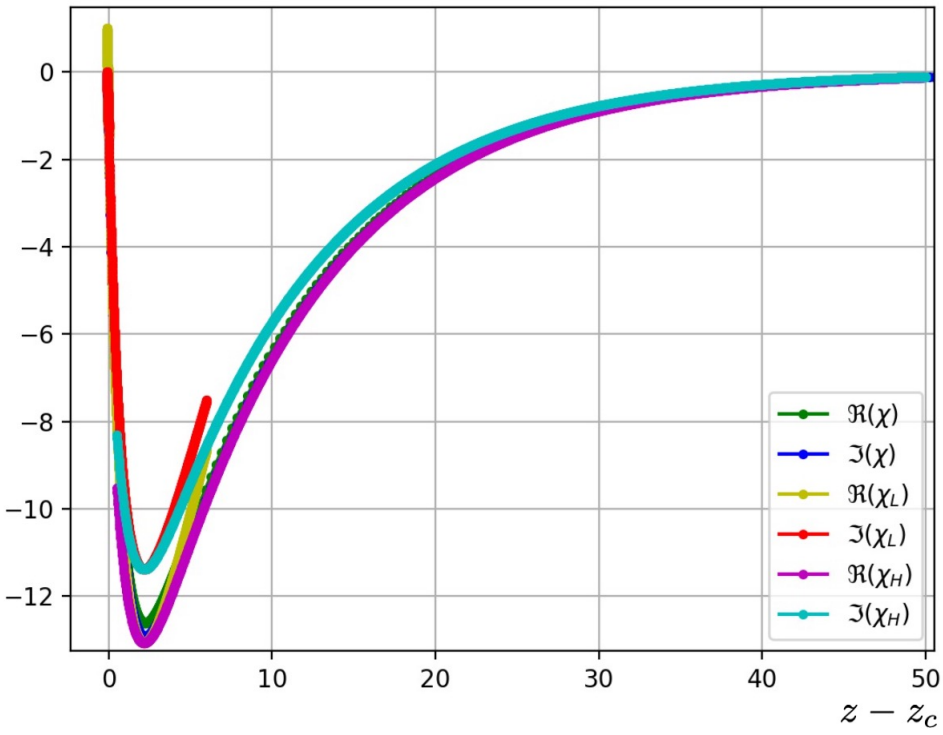

Figure 6.9: Solution for the exponential profile and $k = 0.1$ and $z_c = 0.1$.

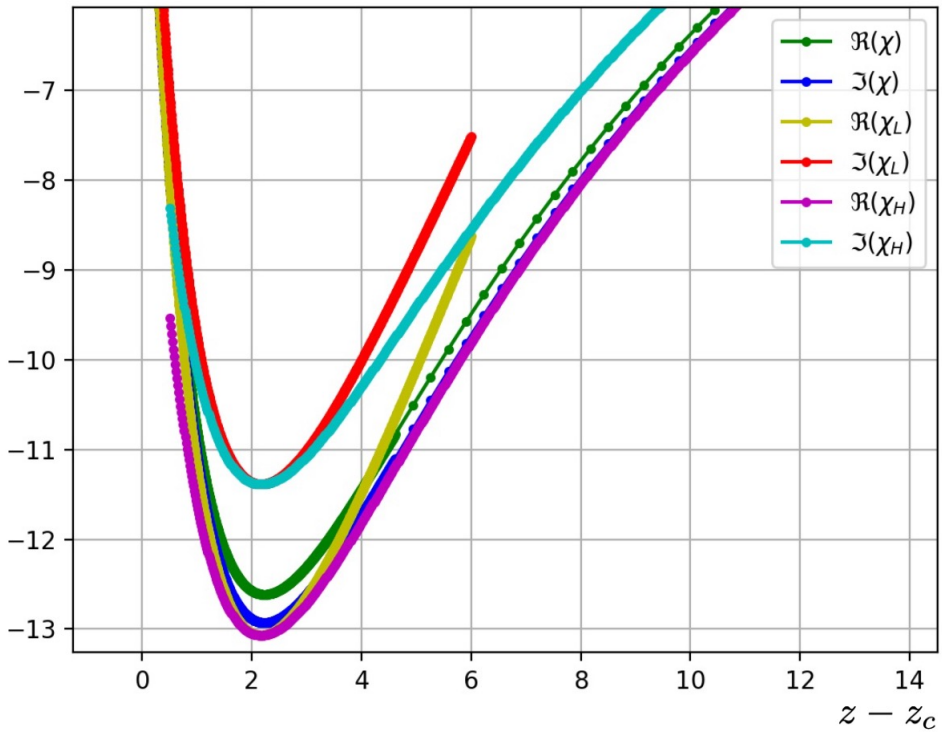

Figure 6.10: Zoom on the minimum (where the patching is made) in figure 6.9.

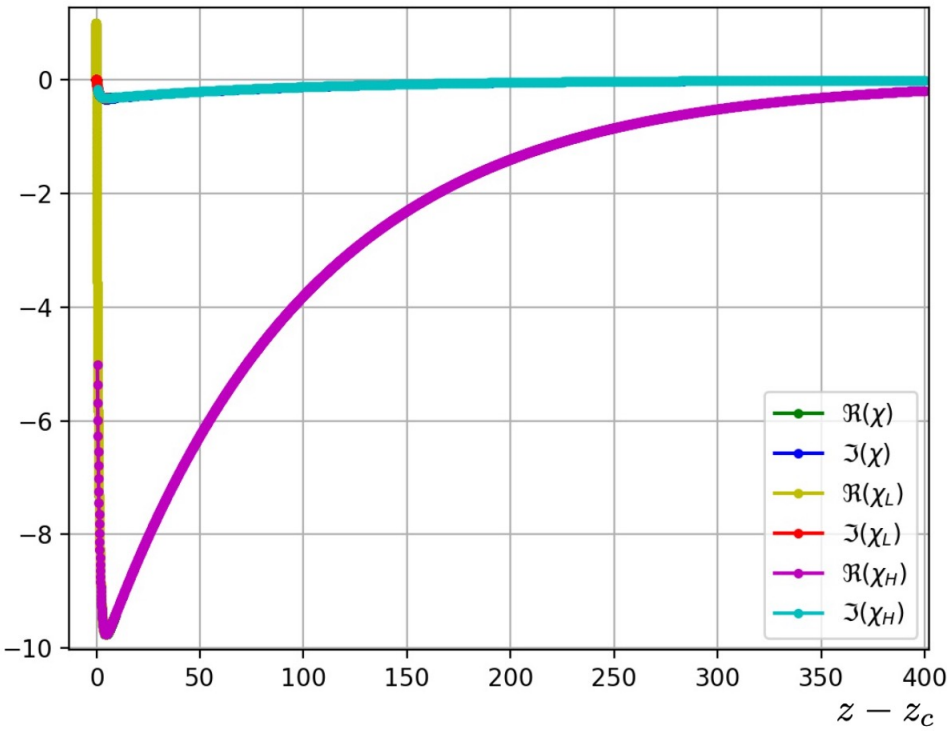

Figure 6.11: Solution for the exponential profile and $k = 0.01$ and $z_c = 0.1$.

Bibliography

[1] A. Lee, D. Vella, and J. S. Wettlaufer. Fluctuation spectra and force generation in nonequilibrium systems. *PNAS; Proceedings of the National Academy of Sciences*, 114(35):9255–9260, 2017.

[2] R. Ni, MAC Stuart, and P.G. Bolhuis. Tunable long range forces mediated by selfpropelled colloidal hard spheres. *Phys Rev Lett*, 114:018302, 2015.

[3] H. B. Casimir. On the attraction between two perfectly conducting plates. *Proc. K. Ned. Akad. Wet.*, 51:793–795.

[4] P. W. Milonni, R. J. Cook, and M. E. Goggin. Radiation pressure from the vacuum: Physical interpretation of the casimir force. *Physical Review A*, 28:1621–1623, 1988.

[5] W.J. Pierson and L. Moskowitz. A proposed spectral form for fully developed wind seas based on the similarity theory of S.A. Kitaigorodskii. *J. Geophys. Res.*, 69:5181–5190, 1964.

[6] A. D. D. Craik. The origins of water wave theory. *Annu. Rev. Fluid Mech.*, 36:1–28, 2004.

[7] I Grattan-Guinness. *Convolutions in French mathematics, 1800-1840.* Springer Basel AG, 1990.

[8] G. B. Airy. Tides and waves. *Encyclopaedia Metropolitana*, Vol. 3, 1841.

[9] A. Sommerfeld. *Mechanics of deformable bodies: Lectures on Theoretical Physics, Volume 2.* Academic Press, 1950.

[10] O. M. Phillips. The equilibrium range in the spectrum of wind-generated water waves. *Journal of Fluid Mechanics*, 4:426–434, 1958.

[11] G. G. Stokes. On the theory of oscillatory waves. *Trans. Camb. Phil. Soc.*, 8:441–455, 1847.

[12] T. Levi-Civita. Détermination rigourese des ondes permanentes d'ampleur finie. *Math. Ann.*, 93:264–314, 1925.

[13] T. B. Benjamin and J. E. Feir. The disintegration of wave trains on deep water. Part I. Theory. *Journal of Fluid Mechanics*, 27:417–430, 1967.

[14] C. Godrèche and P. Manneville. *Hydrodynamics and Nonlinear Instabilities.* Cambridge University Press, 2005.

[15] V. E. Zakharov and L. A. Ostrovsky. Modulation instability: The beginning. *Physica D*, 238:540–548, 2009.

[16] J. T Stuart and R. C. DiPrima. The Eckhaus and Benjamin-Feir resonance mechanisms. *Proc. R. Soc. Lond.*, 362:27–41, 1978.

[17] P. A. E. M. Janssen. *The interaction of ocean waves and wind.* Cambridge University Press, 2004.

[18] V. E. Zakharov. Stability of periodic waves of finite amplitude on the surface of a deep fluid. *J. Appl. Mech. Tech. Phys.*, 9:190–194, 1968.

[19] O. M. Phillips. On the dynamics of unsteady gravity waves of finite amplitude. Part I. The elementary interactions. *Journal of Fluid Mechanics*, 9:193–217, 1960.

[20] A. I. Dyachenko, D. I. Kachulin, and V. E. Zakharov. Super compact equation for water waves. *Journal of Fluid Mechanics*, 828:661–679, 2017.

[21] M. L. Banner and W. K. Melville. On the separation of air flow over water waves. *Journal of Fluid Mechanics*, 77:825–842, 1976.

[22] F. Ursell. Wave generation by wind. *In Surveys in Mechanics, ed. by G. K. Batchelor*, pages 216–249, 1956.

[23] O. M. Phillips. On the generation of waves by turbulent wind. *Journal of Fluid Mechanics*, 2:417–445, 1957.

[24] J. W. Miles. On the generation of surface waves by shear flows. *Journal of Fluid Mechanics*, 3:185–204, 1957.

[25] P. G. Drazin and W. H. Reid. *Hydrodynamic stability*. Cambridge University Press, 1981.

[26] A. S. Monin and A. M. Yaglom. *Statistical fluid mechanics. Mechanics of turbulence. Volume 1.* Dover Publications, 2007.

[27] W. R. Young and C. L. Wolfe. Generation of surface waves by shear-flow instability. *Journal of Fluid Mechanics*, 739:276–307, 2013.

[28] L. C. Morland and P. G. Saffman. Effect of wind profile on the instability of wind blowing over water. *Journal of Fluid Mechanics*, 252:383–398, 1993.

[29] S. D. Conte and J. W. Miles. On the numerical integration of the Orr-Sommerfeld equation. *J. Soc. INDUST. APPL. MATH.*, 7:361–366, 1959.

[30] S. Beji and K. Nadaoka. Solution of Rayleigh's instability equation for arbitrary wind profiles. *Journal of Fluid Mechanics*, 500:65–73, 2004.

[31] T. H. Hughes and W. H. Reid. On the stability of the asymptotic suction boundary-layer profile. *Journal of Fluid Mechanics*, 23:715–735, 1965.

[32] G. B. Arfken, H. J. Weber, and F. E. Harris. *Mathematical methods for physicists*. Academic Press, 2013.

[33] W. J. Plant. A relationship between wind stress and wave slope. *J. Geophys. Res.*, 87(C3):1961–1967, 1982.

[34] H Mitsuyasu and T Honda. Wind-induced growth of water waves. *Journal of Fluid Mechanics*, 123:425–442, 1982.

[35] J. W. Miles. Surface-wave generation revisited. *Journal of Fluid Mechanics*, 256:427–441, 1993.

[36] O. M. Phillips. *The dynamics of the upper ocean*. Cambridge University Press, 1977.

[37] O. M. Phillips. On the dynamics of unsteady gravity waves of finite amplitude. Part II. Local properties of a random wave field. *Journal of Fluid Mechanics*, 11:143–155, 1961.

[38] O. Bühler. *Waves and mean flows*. Cambridge University Press, 2014.

[39] M. W. Dingemans. *Water wave propagation over uneven bottoms*. World Scientific, 1997.

[40] S. Nazarenko. *Wave turbulence*. Springer-Verlag, 2011.

[41] P. A. E. M. Janssen. Quasilinear approximation for the spectrum of wind-generated water waves. *Journal of Fluid Mechanics*, 117:493–506, 1982.